J. Fluid Mech. (1986), *vol.* 166, *pp.* 473–502
Printed in Great Britain

On time-dependent settling of a dilute suspension in a rotating conical channel

By GUSTAV AMBERG,† ANDERS A. DAHLKILD,† FRITZ H. BARK† AND DAN S. HENNINGSON

Department of Mechanics, The Royal Institute of Technology, Stockholm, S-100 44 Sweden

(Received 20 December 1983 and in revised form 6 November 1985)

The time-dependent settling of a dilute monodisperse suspension in a centrifugal force field is considered. The settling takes place between two axisymmetric narrowly spaced conical disks that are rotating rapidly. Clear fluid and suspension are assumed to behave as Newtonian fluids of different densities. The viscosities are, for simplicity, assumed to be the same. All effects of the sediment are neglected. The fluid motion is assumed to be almost parallel with the disks and is computed by using lubrication theory. This leads to a nonlinear hyperbolic equation of first order for the location of the interface between clear fluid and suspension. Local multivaluedness of the solution is removed by inserting shocks. Such a shock is a model for a small region where the slope of the interface, as scaled in the lubrication approximation, is large. Two problems are solved: batch settling and a case where the suspension is pumped into a conical channel that is initially filled with clear fluid. In the batch-settling case, the solution is quite similar to that computed by Herbolzheimer & Acrivos for settling due to a constant gravity field in a narrow tilted channel. For large values of the Taylor number, it is found that the blocking of radial flow outside the Ekman layers leads to a somewhat slower separation process than expected. In the filling problem, the character of the solution is distinctly different for Taylor numbers of order unity and large values of this parameter.

1. Introduction

This paper considers axisymmetric settling of a dilute monodisperse suspension in the centrifugal force field between two narrowly spaced rotating conical disks. Processes of this kind are of importance in separation technology. In many designs for industrial centrifuges (Sokolov 1971, Svarovsky 1981, Hsu 1981) the separation efficiency is significantly enhanced by placing a stack of conical disks in front of the outlet as shown in figure 1. This design seems to have been first proposed by von Bechtholsheim (Patenschrift No. 48615, Klasse 82, Kaiserliches Patentamt, 1889). Because von Bechtholsheim's findings were not published in an archival journal, the discovery of the physical mechanism made use of in his design has instead been ascribed to Boycott (1920). In an experimental study of settling of blood corpuscles in a test-tube, Boycott found that the time for complete separation of particles and fluid is considerably smaller in a tilted tube than in a tube that is aligned with the direction of gravity. The reason is that the tilting of the tube increases the projection on a horizontal plane of the volume of suspension, which will increase the rate of production of clear fluid. Equivalently, one may say that the path of fall of the

† Present address: Department of Hydromechanics, The Royal Institute of Technology, Stockholm, S-10044 Sweden.

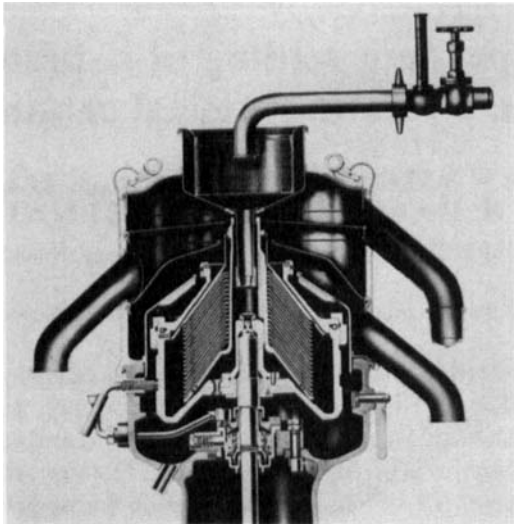

FIGURE 1. Sectional view of an industrial separator with a stack of narrowly spaced conical disks. From *The Evolution of the Alfa-Laval Centrifugal Separator* (Tumba, Sweden: Alfa-Laval AB).

particles in the suspension is decreased in the tilted tube. A thorough discussion of the kinematics of this phenomenon is given by Acrivos & Herbolzheimer (1979).

The first analytical study, based on fundamental principles of fluid mechanics, of effects of inclined walls on settling is the work by Probstein, Yung & Hicks (1977). These authors, who investigated steadily operating lamella settlers, pointed out that not only the clear fluid but also the suspension and the sediment may, in many cases, be regarded as Newtonian fluids of different densities and viscosities. The concentration of suspended material in the suspension was assumed to be constant and the settling velocity was assumed to be given by an empirically modified Stokes law. Probstein *et al.* (1977) also performed experiments and good agreement with theory was found. Further developments of this work have been reported by Leung & Probstein (1983). Several of the basic ideas in the theoretical modelling by Probstein *et al.* (1977) will be used also in the present work.

Time-dependent batch settling was considered by Acrivos & Herbolzheimer (1979) and Herbolzheimer & Acrivos (1981). These studies were both theoretical and experimental. Attention was restricted to moderately dilute suspensions so that effects of the sediment could be ignored in the theoretical analysis, which, to a large extent, otherwise rests on similar assumptions as those made by Probstein *et al.* (1977). Acrivos & Herbolzheimer (1979) investigated settling in vessels with an aspect ratio of order unity and showed, in agreement with the well-known kinematic PNK-model, first proposed by Ponder (1925) and, independently, by Nakamura & Kuroda (1937), that there is a thin layer of clear fluid with boundary-layer-like flow beneath the downward-facing wall of the vessel. Herbolzheimer & Acrivos (1981) studied settling in narrow channels such that the distance between the walls of the channel is of the same order of magnitude as the thickness of the clear-fluid layer. A correction of finite magnitude of the PNK-theory, due to the small distance between the walls of the channel, was computed. The experimental observations in these studies were in good agreement with the theoretical predictions.

Batch settling due to gravity in vessels of aspect ratio $O(1)$, such as those considered by Acrivos & Herbolzheimer (1979), but in a different parameter regime for

the dynamics of the flow, was studied theoretically by Schneider (1982). Roughly speaking, one may say that viscous effects are weaker in the cases studied by Schneider, who showed that this results in a different structure of the motion of both the clear-fluid layer and the suspension. The study by Schneider was also extended to suspensions of quite large concentrations in which propagation of concentration waves is known to occur (Kynch 1952). Experimental verification of Schneider's predictions has been given by Schaflinger (1984).

Theoretical studies of batch settling in rotating containers have been carried out by Greenspan (1983) and Anestis & Schneider (1983). These authors demonstrated that settling in a centrifugal field, which varies in space, is distinctly different from settling in a constant gravitational field. Among other things, the concentration of particles in the suspension can no longer be taken as constant because the settling velocity varies with the distance from the axis of rotation. Both of these studies were concerned with geometries where the phenomena discovered by von Bechtholsheim and Boycott (1920) are of no importance.

The present work is an extension of the theoretical results of Herbolzheimer & Acrivos (1981) in that the channel is rotating rapidly. The constant gravity force is thus replaced by a variable centrifugal force. Furthermore, for small Rossby numbers and moderately large Taylor numbers, which is a common parameter range in applications, rotation adds further significant modifications such as the presence of Ekman layers and regions of nearly inviscid geostrophic flow. A difference of some importance, which has nothing to do with rotation, between the present work and that by Herbolzheimer & Acrivos (1981) is the construction of shocks to remove non-uniqueness of the solution.

The disposition of the paper is the following: §2 contains the formulation of the problem, which partly quite closely follows that given by Acrivos & Herbolzheimer (1979). Batch settling is considered in §3 where the computation of shocks is also discussed in some detail. The behaviour of a suspension that enters a channel, which is initially filled with clear fluid, is considered in §4. The main conclusions of the paper are summarized in §5. The mathematics leading to the results given in §§3 and 4 is, in certain cases, lengthy but straightforward and so parts of the derivations are only briefly described in the text or simply deleted.

2. Formulation

The sedimentation phenomena to be studied take place between two parallel conical disks, whose cone angle is α (see figure 2*a*). The outer edges of the disks are at a distance $l \sin\alpha$ from the axis of symmetry. The gap width between the disks is h and in what follows it is assumed that $h/l \ll 1$. The distance between the inner edges of the disks and the axis of symmetry is $kl \sin\alpha$ where $0 < k < 1$.

The disks rotate with the constant angular velocity Ω around the axis of symmetry. An orthogonal coordinate system (x^*, y^*, θ), where asterisks denote dimensional quantities, will be used (see figure 2*a*). The coordinate system is rotating with the disks. The unit vectors $\boldsymbol{e}_x$ and $\boldsymbol{e}_\theta$ are parallel with the disks and $\boldsymbol{e}_\theta$ is perpendicular to the axis of rotation. $\boldsymbol{e}_y$ is perpendicular to the disks. The origin is where the extension of the outer disk intersects the axis of rotation.

The settling two-phase fluid considered here is a dilute monodisperse suspension of small solid spherical particles (or small incompressible drops) in an incompressible Newtonian fluid. It is assumed, as was done by Probstein *et al.* (1977) and others, that the suspension itself can be regarded as a Newtonian fluid with a viscosity that depends on the local particle concentration. There is experimental evidence that this

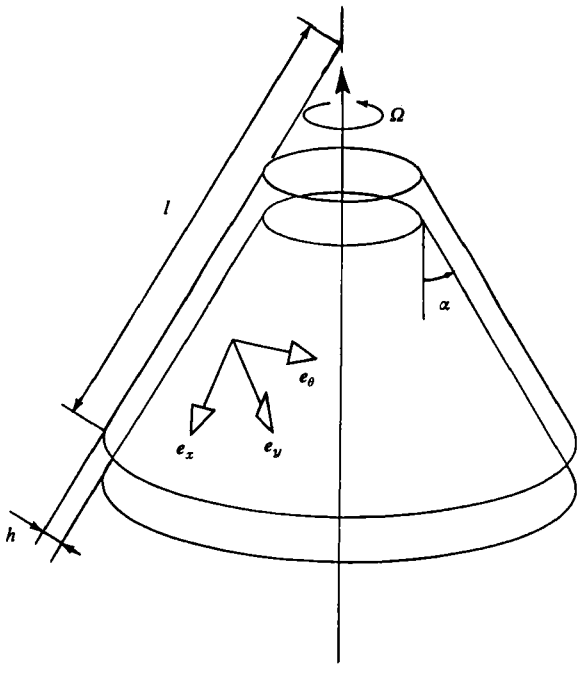

(a)

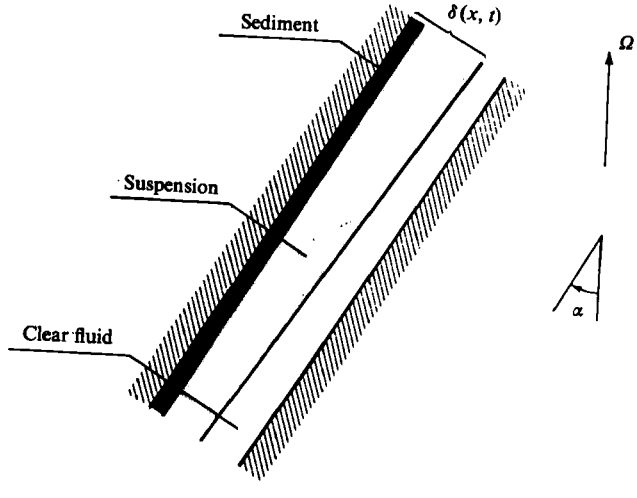

(b)

FIGURE 2. (a) Sketch of conical channel and definition of unit vectors. (b) Sectional view of the channel between the inner and outer disk showing the flow configuration.

approximation is reasonable for particle volume fractions less than 0.3 (Chan & Powell 1984). In terms of the volume-averaged (Drew 1983) or time-averaged (Ishii 1975) velocities $\boldsymbol{u}_p^*, \boldsymbol{u}_f^*$ and densities ρ_p^*, ρ_f^* of the particles and the suspending fluid respectively, the bulk average velocity $\boldsymbol{u}^*$ and density ρ^* of the suspension are defined as

$$[\boldsymbol{u}^*, \rho^*] = (1-c)\,[\boldsymbol{u}_f^*, \rho_f^*] + c[\boldsymbol{u}_p^*, \rho_p^*], \tag{2.1}$$

where c is the volumetric concentration of particles. Conservation of particles and suspending fluid implies that (see e.g. Drew 1983)

$$\frac{\partial c}{\partial t^*} + \nabla^* \cdot (c\boldsymbol{u}_p^*) = 0, \tag{2.2a}$$

$$-\frac{\partial c}{\partial t^*} + \nabla^* \cdot [(1-c)\,\boldsymbol{u}_f^*] = 0. \tag{2.2b}$$

It follows from (2.2a, b) and (2.1) that

$$\nabla^* \cdot \boldsymbol{u}^* = 0. \tag{2.3}$$

The motion of the particles relative to the suspending fluid due to the centrifugal force is assumed to be given by the following empirical expression for the 'slip velocity':

$$\boldsymbol{u}_s^* = \boldsymbol{u}_p^* - \boldsymbol{u}^* = v_S(r^*)\, F\left(\frac{c}{c_0}\right) \boldsymbol{e}_r, \tag{2.4}$$

where $v_S(r^*)$ is the Stokes settling velocity for a single particle at a distance r^* from the axis of rotation. F is a non-dimensional empirically determined function that accounts for particle interactions (Barnea & Mizrahi 1973). c_0 is a reference concentration that will be specified later and $\boldsymbol{e}_r$ is the unit vector in the radial direction. For solid spherical particles

$$v_S(r^*) = \frac{2(\rho_p^* - \rho_f^*)\,(a\Omega)^2\, r^*}{9\mu}, \tag{2.5}$$

where μ is the viscosity of the suspending fluid and a is the particle radius. Equation (2.5) is readily generalized to fluid droplets of a Newtonian fluid (see e.g. Batchelor 1967, p. 236). It should be noted that the effect of concentration on the slip motion, which is described by the function F in (2.4), in the general case leads to propagation of concentration waves in the suspension (Kynch 1952, Schneider 1982). In the present problem, though, as well as in the closely related problems considered by, e.g. Herbolzheimer & Acrivos (1981) and Leung & Probstein (1983), it becomes apparent, as will be discussed later, that such waves do not appear. Therefore, the function F only appears as a numerical correction of the Stokes settling velocity and can be absorbed in the scaling (see (2.27a, b) below).

The slip motion of the particles in the direction of the centrifugal force leads to the formation of a layer of clear fluid adjacent to the inner disk, see figure 2(b). The interface between clear fluid and suspension is denoted $y^* = \delta^*(x^*, t^*)$. On the outer disk, particles will accumulate and form a layer of sediment. This layer is heavier than the suspension and will thus tend to move radially outwards owing to the centrifugal force. In general, the sediment layer may therefore exert a shear stress on the suspension. However, if the sediment layer is thin, which would be the case for dilute suspensions, this effect can on reasonable grounds be expected to be weak. Following Herbolzheimer & Acrivos (1981), this is assumed to be the case in what follows. (Other possible effects of the sediment layer will be discussed later.) Some brief comments on the validity of this assumption may be in order. For the dilute suspensions of rigid spheres investigated experimentally by Herbolzheimer & Acrivos (1981), justification is provided by the good agreement between theory and experiment.† In the case of suspensions of droplets, no experimental information seems to

† Some crude, exploratory tests carried out by the authors for a non-rotating narrow channel, also confirm that the sediment has little effect on the flow.

be available. However, if one assumes that the drops in the sediment layer coalesce and form a layer of a Newtonian fluid with a viscosity that is of the same order of magnitude as that of the suspension, some theoretical estimates can be made. The details are lengthy and not given here. For the parameter range considered in the present work, which is specified by (2.6) and (2.7) below, one finds that the errors in the solutions given in §§3 and 4 are $\sim c$ and $\sim c^{\frac{3}{2}}$ respectively.

Another simplification, which is also taken from Herbolzheimer & Acrivos (1981), is that the viscosities of the clear fluid and the suspension are assumed to be the same. For small concentrations this is justified by Einstein's formula. For moderately small concentrations, $c_0 = 0.1$ say, the validity of this assumption may be disputable. On the other hand, it seems to be very unlikely that a relative difference in viscosity of moderate magnitude will introduce any essential new physical effect. In fact, the good agreement between theory and experiment in the work by Herbolzheimer & Acrivos (1981) indicates strongly that the difference in viscosity between clear fluid and suspension is of minor importance, even for moderately small concentrations.

The following non-dimensional parameters will be used:

$$\left.\begin{aligned} &\Lambda = \frac{c_0(\rho_p^* - \rho_f^*)\, l^3 \Omega^2}{\mu v_S(l)} = \tfrac{9}{2} c_0 \left(\frac{l}{a}\right)^2, \\ &\text{Reynolds number:} \quad R = \frac{\rho_0^* v_S(l)\, h}{\mu}, \\ &\text{Taylor number:} \quad T = \frac{\rho_0^* \Omega h^2 \sin\alpha}{\mu}, \end{aligned}\right\} \tag{2.6}$$

where μ is the viscosity and $\rho_0^* = \rho^*(c_0)$. Λ is an estimate of the ratio between buoyancy forces ($\sim c_0(\rho_p^* - \rho_f^*) l\Omega^2$) and viscous forces ($\sim \mu v_S / l^2$) that are caused by shear on the lengthscale l. In most applications, Λ is very large; values of order 10^7 are common. The appearance of boundary-layer-like flows in containers that are characterized by a single lengthscale l is a consequence of the fact that Λ is very large. Typical orders of magnitude of the Reynolds and Taylor numbers are, in many practical cases, $R \ll 1$ and $T \sim 1$ or larger. The reason why centrifuges are designed in this way is that the efficiency of the machine increases as the retention time of the particles in the suspension decreases. For a given size of centrifuge, the efficiency will thus increase with the number of disks, i.e. decreasing values of h, and, of course, with increasing values of Ω. The flow between the disks is therefore often such that viscous forces, due to the narrow spacing, dominate inertial forces except for the Coriolis force, which may be significant due to the rapid rotation. For typical numbers and a more thorough discussion of technical details, the reader is referred to the engineering text-books by Sokolov (1971), Svarovsky (1971) and Hsu (1981). In summary, the following parameter regime will be considered in the present work:

$$\Lambda^{-1} \ll 1, \quad R \ll 1, \quad T \gtrsim 1. \tag{2.7}$$

The distance between the disks is assumed to be small in the following sense:

$$\frac{h}{l} = \hat{h}\Lambda^{-\frac{1}{3}}, \quad \hat{h} \sim 1, \tag{2.8}$$

which is often the case in applications. If Coriolis effects are negligible, this is the limit in which viscous forces are of the same order of magnitude as buoyancy forces across the whole channel.

The following scales will be used:

$$\left.\begin{array}{ll} \text{time} & h/v_{\mathrm{S}}(l), \\ \text{length in the } \boldsymbol{e}_y \text{ direction} & h, \\ \text{length in the } \boldsymbol{e}_x \text{ direction} & l, \\ \text{velocity in the } \boldsymbol{e}_y \text{ direction} & v_{\mathrm{S}}(l), \\ \text{velocity in the } \boldsymbol{e}_x \text{ and } \boldsymbol{e}_\theta \text{ directions} & \Lambda^{\frac{1}{3}} v_{\mathrm{S}}(l)/\hat{h}, \\ \text{reduced pressure} & \Lambda \mu v_{\mathrm{S}}(l)/l\hat{h}^2, \\ \text{concentration} & c_0, \\ \text{density} & \rho_0^*. \end{array}\right\} \tag{2.9}$$

The non-dimensional radius and bulk-velocity vectors and the gradient operator are thus given by the following expressions:

$$\left.\begin{aligned} \boldsymbol{x} &= x\boldsymbol{e}_x - \Lambda^{-\frac{1}{3}}\hat{h}y\boldsymbol{e}_y, \\ \boldsymbol{u} &= u_x\boldsymbol{e}_x + \Lambda^{-\frac{1}{3}}\hat{h}u_y\boldsymbol{e}_y + u_\theta\boldsymbol{e}_\theta, \\ \boldsymbol{\nabla} &= \Lambda^{-\frac{1}{3}}\hat{h}\boldsymbol{e}_x\frac{\partial}{\partial x} + \boldsymbol{e}_y\frac{\partial}{\partial y}. \end{aligned}\right\} \tag{2.10}$$

Unless explicitly stated otherwise, in the following all quantities are dimensionless.

The equation of continuity for the suspended particles (2.2*a*) can be written in the following form

$$\frac{\partial\phi}{\partial t} + [\boldsymbol{u} + (F + \phi F')\boldsymbol{u}_{\mathrm{s0}}]\cdot\boldsymbol{\nabla}\phi = -2\Lambda^{-\frac{1}{3}}\hat{h}\phi F, \tag{2.11}$$

where ϕ is the concentration and $\boldsymbol{u}_{\mathrm{s0}}$ is the slip velocity for zero concentration. In the derivation of (2.11), use has been made of the relation

$$\boldsymbol{\nabla}\cdot\boldsymbol{u}_{\mathrm{s0}} = 2\Lambda^{-\frac{1}{3}}\hat{h}. \tag{2.12}$$

The characteristic form of (2.11) is

$$\frac{\mathrm{d}\phi}{\mathrm{d}t} = -2\Lambda^{-\frac{1}{3}}\hat{h}\phi F, \tag{2.13a}$$

$$\frac{\mathrm{d}\boldsymbol{x}}{\mathrm{d}t} = \boldsymbol{u} + (F + \phi F')\boldsymbol{u}_{\mathrm{s0}}. \tag{2.13b}$$

The velocity of concentration waves $\mathrm{d}\boldsymbol{x}/\mathrm{d}t$ is precisely the local bulk velocity $\boldsymbol{u}$ plus the wave speed in the absence of bulk motion. Thus (2.13*b*) simply means that concentration waves, which were first discussed by Kynch (1952), are advected by the local bulk velocity. The small term in the right-hand side of (2.13*a*) implies that for $t \sim 1$, the concentration decreases slightly along the characteristic curves defined by (2.13*b*). The reason is that the velocity field $\boldsymbol{u}_{\mathrm{s0}}$ is divergent (see 2.12), i.e. the particle cloud behaves like an expanding gas. However, on the timescale considered, the concentration variation is only $\sim \Lambda^{-\frac{1}{3}}$. If the suspension is initially of uniform concentration, it will therefore approximately remain so. Only cases such as these will be considered in the present work and henceforth the approximate value $\phi = 1$ will be used for the concentration in the suspension. For $\hat{h} \sim \Lambda^{\frac{1}{3}}$, i.e. in a channel of aspect ratio ~ 1, one would have to account for a finite variation of the

concentration. Problems where this is the case have been considered by Greenspan (1983) and Anestis & Schneider (1983).

The presence of an interface $y = \delta(x,t)$ between suspension and clear fluid, across which ϕ changes discontinuously, has not been accounted for in the previous arguments. Such an interface, which is a kinematic shock, may be unstable and thereby act as a source for concentration waves. (This type of instability has nothing to do with the hydrodynamic stability of the bulk motion.) In settling without bulk motion, this situation is known to prevail under certain circumstances for the interface between suspension and sediment (Kynch 1952, Schneider 1982, Anestis & Schneider 1983) and so is worth some consideration.

The stability condition for a kinematic shock $y = \chi(x,t)$, say, that separates two regions of concentrations ϕ_1 and ϕ_2 respectively, is locally the same as if the bulk motion were absent.† This follows directly from the aforementioned result that concentration waves are locally advected by the bulk velocity, which is continuous across a shock. The physical reason is, of course, that the slip velocity is independent of the bulk velocity. The stability condition is thus locally the same as that given by Kynch (1952). A more general necessary and sufficient stability condition for shocks of this type has been given by, among others, Lax (1973). In terms of the unit normal vector

$$\boldsymbol{n} = \left(\frac{\partial \chi}{\partial x}, -1\right)\left[1+\left(\frac{\partial \chi}{\partial x}\right)^2\right]^{-\frac{1}{2}}$$

and the function $f(\phi) = \phi F(\phi)$, Lax's condition can be written

$$\boldsymbol{n}\cdot\boldsymbol{u}_{s0}\frac{f(\phi)-f(\phi_2)}{\phi-\phi_2} \leqslant \boldsymbol{n}\cdot\boldsymbol{u}_{s0}\frac{f(\phi_1)-f(\phi_2)}{\phi_1-\phi_2} \leqslant \boldsymbol{n}\cdot\boldsymbol{u}_{s0}\frac{f(\phi)-f(\phi_1)}{\phi-\phi_1} \tag{2.14}$$

for $\phi_1 \leqslant \phi \leqslant \phi_2$ and where $\phi_{1,2}$ are chosen such that $\boldsymbol{n}$ points into the region of concentration ϕ_2. If the density stratification is stable, i.e. $\boldsymbol{n}\cdot\boldsymbol{u}_{s0} > 0$, the geometrical interpretation of (2.14) is that the secant between the points $(\phi_1, f(\phi_1))$ and $(\phi_2, f(\phi_2))$ is everywhere below the curve $f(\phi)$. This seems to always be the case for the clear fluid–suspension interface. Concentration waves from the interface between suspension and sediment were investigated in detail by Schneider (1982), who showed that such waves do not occur if the volumetric concentration $c_0 \lesssim 0.15$. This will be assumed to be the case in what follows.

It should be noted, though, that a non-zero bulk flow in principle may cause concentration waves to appear by folding of an interface over itself. This would lead to an unstable density stratification (with $\boldsymbol{n}\cdot\boldsymbol{u}_{s0} < 0$) along some part of the interface, which would then disintegrate by waves of 'expansion' type. (The unstable density stratification would presumably also lead to hydrodynamic instability of the motion). In the present work, however, only stably stratified flows occur.

Before the dynamics of the flow is considered some kinematical relations involving shocks will be derived for later use. Conservation of suspended particles across a shock gives the following Rankine–Hugoniot relation

$$\phi_1(\boldsymbol{n}\cdot\boldsymbol{u}_{p1} - U) = \phi_2(\boldsymbol{n}\cdot\boldsymbol{u}_{p2} - U), \tag{2.15}$$

where

$$U = \frac{\partial \chi}{\partial t}\Big/\left[1+\left(\frac{\partial \chi}{\partial x}\right)^2\right]^{\frac{1}{2}} \tag{2.16}$$

† It will turn out later that regions where the slope of the interface is locally very large need special consideration. This matter is discussed at the end of this section.

is the velocity of the shock. Combination of the non-dimensional version of (2.4) and (2.15) gives

$$U = \boldsymbol{n}\cdot\boldsymbol{u} + \boldsymbol{n}\cdot\boldsymbol{u}_{s0}\frac{f(\phi_2)-f(\phi_1)}{\phi_2-\phi_1}. \tag{2.17}$$

If one takes the limits $\phi\to\phi_1$ and $\phi\to\phi_2$ in (2.14), adds $\boldsymbol{n}\cdot\boldsymbol{u}$ to each member and combines the result with (2.13*b*) and (2.17), one finds

$$\boldsymbol{n}\cdot\frac{\mathrm{d}\boldsymbol{x}}{\mathrm{d}t}\bigg|_{\phi=\phi_2} \leqslant U \leqslant \boldsymbol{n}\cdot\frac{\mathrm{d}\boldsymbol{x}}{\mathrm{d}t}\bigg|_{\phi=\phi_1}. \tag{2.18}$$

This necessary condition for stability means that characteristics should either be directed into, or be tangential to, the shock path.

The non-dimensional equations for conservation of momentum and mass for the bulk motion are (with $\phi = 1$ for $y < \delta$, $\phi = 0$ for $y > \delta$)

$$\Lambda^{\frac{1}{3}}R\rho(\phi)\frac{\mathrm{D}\boldsymbol{u}}{\mathrm{D}t} + \frac{2T\rho(\phi)}{\sin\alpha}\boldsymbol{e}_z\times\boldsymbol{u} = -\nabla\Pi - \nabla\times\nabla\times\boldsymbol{u} - (1-\phi)\,\boldsymbol{e}_z\times(\boldsymbol{e}_z\times\boldsymbol{x}), \tag{2.19a}$$

$$\nabla\cdot\boldsymbol{u} = 0, \tag{2.19b}$$

where $\boldsymbol{e}_z = \boldsymbol{\Omega}/|\boldsymbol{\Omega}|$ and the non-dimensional reduced pressure Π is defined in terms of the dimensional pressure p^* as

$$\Pi = \frac{lh^2}{\Lambda\mu v_S(l)}(p^* - \tfrac{1}{2}\rho_0^*|\boldsymbol{\Omega}\times\boldsymbol{x}^*|^2). \tag{2.20}$$

Simplification of (2.19*a*) is necessary. It follows from (2.10) that $|\mathrm{D}\boldsymbol{u}/\mathrm{D}t| \sim \Lambda^{-\frac{1}{3}}$. The convective acceleration is thus $\sim R \ll 1$ and can be neglected. The variation of the density with ϕ in the Coriolis force will also be neglected (cf. the Boussinesq approximation), i.e. $\rho(\phi) = 1$ in what follows. Substitution of (2.10) for $\boldsymbol{x}$, $\boldsymbol{u}$ and ∇ gives, to lowest order in $\Lambda^{-\frac{1}{3}}$, the following approximate version of the system (2.19*a*, *b*):

$$-2Tu_\theta = -\frac{\partial\Pi}{\partial x} + \frac{\partial^2 u_x}{\partial y^2} - (1-\phi)\,x\hat{h}^3\sin^2\alpha, \tag{2.21a}$$

$$0 = -\frac{\partial\Pi}{\partial y}, \tag{2.21b}$$

$$2Tu_x = \frac{\partial^2 u_\theta}{\partial y^2}, \tag{2.21c}$$

$$\frac{1}{x}\frac{\partial}{\partial x}xu_x + \frac{\partial u_y}{\partial y} = 0. \tag{2.21d}$$

If the velocity and pressure fields in the clear fluid are denoted by the superscript c and the corresponding quantities in the suspension by the superscript s, the boundary conditions for the solution of (2.21*a–d*) can be written

$$\boldsymbol{u}^s = 0, \quad y = 0, \quad \boldsymbol{u}^c = 0, \quad y = 1, \tag{2.22a}$$

$$\boldsymbol{u}^s = \boldsymbol{u}^c, \quad y = \delta, \tag{2.22b}$$

$$\frac{\partial}{\partial y}(u_x^s, u_\theta^s) = \frac{\partial}{\partial y}(u_x^c, u_\theta^c), \quad y = \delta, \tag{2.22c}$$

$$\Pi^s = \Pi^c, \quad y = \delta. \tag{2.22d}$$

Equations (2.22c, d) are the lowest-order approximations of the continuity conditions for normal and shear stresses across the interface.

If δ is regarded as known, it is straightforward to calculate the velocity field in terms of the pressure field from (2.21a)–(2.22d). The pressure field is determined by specifying the total volume flux in the channel

$$2\pi x \sin\alpha \left(\int_0^{\delta} u_x^{\mathrm{s}} \, \mathrm{d}y + \int_{\delta}^{1} u_x^{\mathrm{c}} \, \mathrm{d}y \right) = Q. \tag{2.23}$$

Owing to the approximations made in the derivation of (2.21a–c), which are the same as those made in lubrication theory, no derivatives with respect to x appear to lowest order. No boundary conditions for the velocity field can therefore be imposed at $x = k, 1$. It has thus been implicitly assumed that the flow adjusts itself to lubrication flow in boundary-layer-like corner regions of length $\sim A^{-\frac{1}{3}}$ at the ends of the plates (cf. DiPrima 1969).

If the velocity field is known in terms of δ, which is so far unknown, an equation for δ can be derived from the lowest-order approximations of (2.16) and (2.17) with $\phi_2 = 1$ and $\phi_1 = 0$. The result is

$$\frac{\partial \delta}{\partial t} + u_x^{\mathrm{s}} \frac{\partial \delta}{\partial x} = u_y^{\mathrm{s}} - \tfrac{1}{2} x F(1) \sin 2\alpha. \tag{2.24}$$

It should be noted that the slip velocity in the x-direction, which is a factor $A^{-\frac{1}{3}}$ smaller than the bulk velocity in the same direction, has been neglected in (2.24).

Instead of using the velocity components $u_{x,y}^{\mathrm{s}}$ in (2.24), a more convenient form can be obtained in terms of the local volume flux of suspension

$$q(x, \delta(x,t)) = 2\pi x \sin\alpha \int_0^{\delta} u_x^{\mathrm{s}} \, \mathrm{d}y. \tag{2.25}$$

Some properties of the function q should be noted. It can be shown that q can be written

$$q = x^2 q_{\mathrm{B}}(\delta) + Q q_Q(\delta), \tag{2.26}$$

where the functions q_{B} and q_Q have simple physical interpretations, cf. Leung & Probstein (1983). (The algebraic expressions are complicated and are therefore given in the Appendix.) In batch settling, the ends of the channel are closed and $Q = 0$. The fluid motion that corresponds to the volume flux $x^2 q_{\mathrm{B}}$ is driven by the difference in density between the suspension and the clear fluid. This motion can be characterized as long, viscous gravity waves of finite amplitude. Velocity profiles u_x and u_θ for a case where Coriolis effects are significant, i.e. a rather large value of T, are shown in figure 3. For reasons that are discussed later, no graph of u_y is shown. The flow consists of three Ekman layers, one at each solid surface and one at the interface, that are separated by regions of inviscid geostrophic flow. For general properties of Ekman layers and geostrophic flows, the reader is referred to the monograph by Greenspan (1968). The function $q_{\mathrm{B}}(\delta)$ is shown in figure 5 for different values of T.

The velocity field corresponding to the volume flux Qq_Q is the same as that for the flow of a homogeneous fluid that is driven by a difference in pressure between the ends of the disks. This velocity field, which can be described as a rotation-modified Poiseuille flow ($u_y = 0$), is thus independent of the location of the interface. Typical velocity profiles are shown in figure 4. In this case only two Ekman layers appear. Figure 12 shows $q_Q(\delta)$ for different values of T.

It should be pointed out that, for large but finite values of T, the lubrication

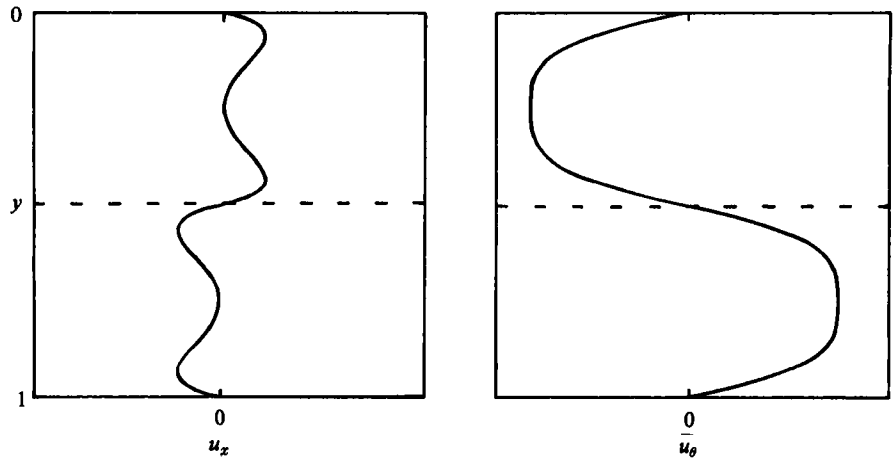

FIGURE 3. Velocity profiles for the batch case ($Q = 0$). The location of the interface is denoted by – – –. $\delta = 0.5$, $T = 144$.

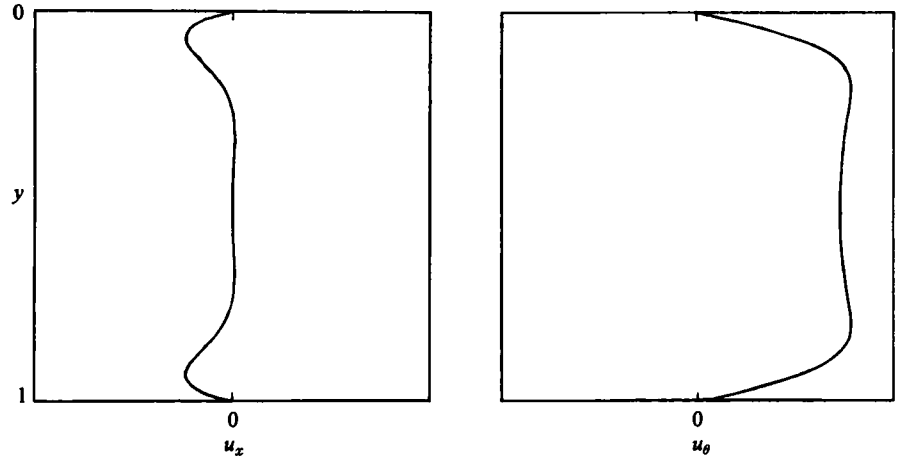

FIGURE 4. Velocity profiles for the filling problem. $Q < 0$, $|Q| \sim 1$, $\epsilon \ll 1$, $T = 144$.

approximation does not, in general, give a correct description of the geostrophic flow (Bark, Johansson & Carlsson 1984). One finds that the Taylor–Proudman theorem (see Greenspan 1968, p. 2) is violated. In the lubrication approximation, the velocity and pressure fields outside the Ekman layers are independent of y whereas these quantities, according to the Taylor–Proudman theorem, should be constant along the direction of $\boldsymbol{e}_z$. For $\hat{h} \sim 1$, however, it can be shown that this leads to relative errors in u_x, u_θ and p of order $A^{-\frac{1}{3}}$. The velocity component u_y on the other hand is incorrect to lowest order. Fortunately, this velocity component is small and a detailed analysis, which is tedious and therefore not given here, shows that this leads to an error $\sim A^{-\frac{1}{3}}$ in the results given later in this paper.

By expressing the velocity components in terms of q, using the normalized variables

$$\bar{t} = \tfrac{1}{2}[F(1)\sin 2\alpha]\,t, \tag{2.27a}$$

$$\bar{q} = \frac{q}{\pi F(1)\sin 2\alpha\cos\alpha}, \tag{2.27b}$$

and dropping overbars one finds that (2.24) can be written

$$\frac{\partial \delta}{\partial t}+\frac{1}{x}\frac{\partial q(x,\delta(x,t))}{\partial x}=-x. \tag{2.28}$$

This type of equation has received much attention in the literature on kinematic waves, which were first studied by Lighthill & Whitham (1955). For later reviews of the subject the reader is referred to Whitham (1974) and Kluwick (1977).

The characteristic form of (2.28) is

$$\frac{\mathrm{d}\delta}{\mathrm{d}t}=-x-\frac{1}{x}\left(\frac{\partial q}{\partial x}\right)_{\delta}, \tag{2.29a}$$

$$\frac{\mathrm{d}x}{\mathrm{d}t}=\frac{1}{x}\left(\frac{\partial q}{\partial \delta}\right)_{x}. \tag{2.29b}$$

Using the expression (2.26) for q, one finds the following solution of (2.29a, b):

$$x^3-x_i^3+3Q[q_Q(\delta)-q_Q(\delta_i)]+x^2q_B(\delta)-x_i^2q_B(\delta_i)=0, \tag{2.30a}$$

$$t-t_i=\int_{\delta_i}^{\delta}\frac{\mathrm{d}\delta'}{x(\delta')+2q_B(\delta')}, \tag{2.30b}$$

where δ_i is the prescribed value of δ at the point $t=t_i$, $x=x_i$. This specification of δ_i needs some consideration.

Two problems will be solved in the present work. The first is batch settling and the second is the setting up of a continuous settling process by pumping a homogeneous suspension into a channel that is initially filled with clear fluid. In the second problem, which will henceforth be referred to as the filling problem, the suspension enters the channel from the outer end. In both of these problems, one obviously has to prescribe δ on $t=0$, $k\leqslant x\leqslant 1$. However, as will be apparent from the next two sections, one also has to prescribe δ at $x=1$ for all values of t. Otherwise only a part of the region $t>0$, $k\leqslant x\leqslant 1$ is accessible for characteristics, i.e. the problem would be ill-posed. For the batch settling problem, Acrivos & Herbolzheimer (1979) showed, by using order-of-magnitude arguments for the velocity components in the outer end region, that one must require

$$\delta(1,t)=1. \tag{2.31}$$

Also, in the filling problem, where the whole channel cross-section at the outer end contains suspension for all values of t, (2.31) must be prescribed as a boundary condition.

The following initial conditions are prescribed.

I. Batch settling problem

$$\delta(x,0)=1,\, k<x\leqslant 1;\quad 0\leqslant\delta(k,0)\leqslant 1. \tag{2.32a}$$

II. Filling problem

$$\delta(x,0)=0,\, k\leqslant x<1;\quad 0\leqslant\delta(1,0)\leqslant 1. \tag{2.32b}$$

The second part of (2.32a) may at first sight seem peculiar. It means that one prescribes an infinitesimally thin region ($0<y<1$, $k<x<k+0$) of clear fluid at the inner end of the channel. Physically, this can have no effect on either the settling or the bulk motion in the channel. However, the mathematical formulation of the problem should include the effect of the closed end at $x=k$. Due to the properties

of the characteristics, which are discussed in detail in the next section, one finds that no *boundary* condition can be prescribed at $x = k$. The effect of the closed end must consequently appear in the *initial* condition and (2.32*a*) is the proper formulation in the present problem. Exactly the same situation arises in the problem for settling due to gravity without bulk motion, which was first considered by Kynch (1952). In that problem, the presence of a horizontal boundary is accounted for by prescribing an infinitesimal layer of sediment on the boundary at the initial instant. It should be pointed out that imposing (2.32*a*) is only formally different from the treatment of the closed end by Herbolzheimer & Acrivos (1981).

The formulation of the initial condition (2.32*b*) for the filling problem is straightforward. Regardless of the details of the flow in the inlet region at the outer end, which is especially complex if Coriolis effects are significant (cf. Ungarish & Greenspan 1984), the variation of the interface will initially appear as a discontinuity in the lubrication approximation.

As is indicated by (2.32*a*, *b*), kinematic shocks will appear in the solution of (2.28). Such a shock in δ is, of course, also a shock for the solution $\phi(x,t)$ of (2.11). Unfortunately, the necessary stability criterion (2.18) for a shock in ϕ is, in general, *not* fulfilled at a shock in δ even if (2.14) is fulfilled. The reason is that the bulk velocity is discontinuous across a shock in δ. However, this discrepancy is a harmless consequence of the use of the lubrication approximation for the computation of the bulk motion. A shock in δ should be regarded as a simplified model for a local continuous variation of δ on the lengthscale h (or any other lengthscale that is significantly smaller than l). The bulk velocity associated with such a variation of δ is, of course, continuous and the shock in ϕ will be stable, provided that the interface does not fold over itself. It is henceforth assumed that this is the case. For low Reynolds numbers, which are assumed to prevail in the present work, this rather strong assumption can be given some justification if Coriolis effects and geometrical effects due to circumferential curvature are neglected and the settling velocity is taken as constant, as in the non-rotating case considered by Herbolzheimer & Acrivos (1981). These restrictions are made only for mathematical simplicity; there seems to be no physical or mathematical reason why the argument should not be valid also for the case considered in the present work. The problem considered by Herbolzheimer & Acrivos is recovered from (2.28) by putting $T = 0$ and $x = 1$ everywhere except in $\delta(x,t)$. If the next term in the expansion for long waves is included in the derivation (see e.g. Kluwick 1977), one finds an equation of the form†

$$\frac{\partial\delta}{\partial t}+\frac{\partial q(\delta)}{\partial x} = -1+\frac{h}{l}\frac{\partial}{\partial x}\left[(\tan\alpha)\,q(\delta)\,\frac{\partial\delta}{\partial x}-(\operatorname{cotan}\alpha)\,\delta\right], \tag{2.33}$$

where $q(\delta) = \frac{1}{3}\delta^3(1-\delta)^3$. This equation has been solved numerically for small values of h/l in some test cases. As can be expected, the solution of the hyperbolic equation (2.28), in the special case described above, approximates, with an error $O(h/l)$, the solution of the parabolic equation (2.33) for $\partial\delta/\partial x \ll 1$. A shock in the solution of (2.28) appears in the solution of (2.33) as a rapid but continuous variation of δ such that the stratification is stable. Thus, in the limit $h/l \to 0$, solutions of the more realistic equation (2.33) seem to reduce to the discontinuous solutions of equation (2.28) in such a way that the jump in ϕ can be regarded as a stable shock also at a shock in δ.

† The derivation of (2.33) and the computations leading to the conclusions outlined above have been carried out by C. Johansson (private communication). This will be reported on elsewhere.

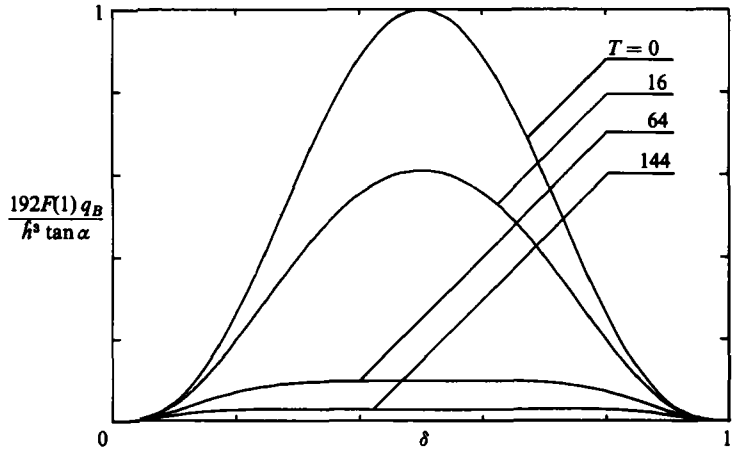

FIGURE 5. The function $q_B(\delta)$ for some values of T.

3. Batch settling ($Q = 0$)

The exact solution (2.30a, b) with δ_l, x_l and t_l chosen such that (2.31) and (2.32a) are fulfilled is quite complicated. However, one can find an approximate but physically more transparent solution. The basis for the approximation is that, for $\hat{h} \sim 1$ and $\tan\alpha \sim 1$, the numerical values of q_B, the local volume flux of suspension, and its lowest-order derivatives with respect to δ are fortuitously small. This is somewhat surprising because these quantities have been scaled to be of order unity. Figure 5 shows q_B as function of δ for various values of T.

It can be shown that

$$\frac{\partial q_B}{\partial T} < 0 \tag{3.1a}$$

and thus

$$q_B < \max\{q_B(\delta, T=0)\} = \frac{\hat{h}^3\tan\alpha}{F(1)}\max\{\tfrac{1}{3}\delta^3(1-\delta)^3\} = \frac{\hat{h}^3\tan\alpha}{192F(1)}. \tag{3.1b}$$

For the large values of T, $\max\{q_B\}$ has the following asymptotic behaviour:

$$\max\{q_B\} = \frac{(1+e^{-\pi})\hat{h}^3\tan\alpha}{4T^{\frac{4}{3}}F(1)} + O(T^{-2}). \tag{3.1c}$$

For a given value of T, one can define the following quantities:

$$\epsilon = \max\{q_B\} \ll 1, \quad \hat{q}_B = \frac{q_B}{\epsilon} \sim 1, \tag{3.2}$$

and assume that δ and x can be expanded in powers of ϵ:

$$(\delta, x) = \sum_{l=0}^{N-1} \epsilon^l(\delta_l, x_l) + O(\epsilon^N). \tag{3.3}$$

Some comments on the circumstances under which ϵ is not small should be made. According to (3.1b) this is the case if the product $\hat{h}^3\tan\alpha$ is large, i.e. the channel is wide and/or the walls of the channel are nearly perpendicular to the axis of rotation. The reason why ϵ increases with $\hat{h}$ for fixed value of $\alpha \neq \frac{1}{2}\pi$ is simply that the

t	exact δ	approx. δ	exact x	approx. x
0.05	0.9750	0.9750	0.4999	0.4999
0.45	0.7700	0.7704	0.4664	0.4664
0.90	0.5067	0.5139	0.4174	0.4175
1.35	0.2418	0.2479	0.4631	0.4660
1.80	0.0109	0.0082	0.4999	0.5069

TABLE 1. Numerical comparison between (2.30a, b) and (3.4a, b) for $k = 0.5$, $T = 4$, $\epsilon = 0.10$

lengthscale for the shear increases. The buoyancy forces, which are driving the motion, are of the same order of magnitude independently of $\hat{h}$. The viscous forces, on the other hand, decrease with increasing values of $\hat{h}$, which results in an increased volume flux of suspension. The limit $\hat{h} \sim 1$ and $\alpha \to \frac{1}{2}\pi$ is spurious. It means that the interface is perpendicular to the walls of the channel. No buoyancy-driven flow will occur at all and the problem formulation in the previous section does not make sense. Henceforth only cases where $\hat{h} \sim 1$ and $\tan\alpha \sim 1$ will be considered.

The fact that q_B, and hence ϵ, decreases with increasing values of T (see 3.1a) has a simple physical interpretation. For large values of T, this is a consequence of the splitting, due to Coriolis effects, of the flow into Ekman layers of thickness $\sim T^{-\frac{1}{2}}$ and regions of inviscid geostrophic flow as shown in figure 3. It can readily be shown that the large viscous shear force in the Ekman layers at the walls causes the velocity field to be weaker by a factor $\sim T^{-1}$ compared with cases where $T \sim 1$ or smaller. Furthermore, because the flow is axisymmetric, no radial volume flux is carried by the geostrophic flow (Greenspan 1968, p. 108). The radial transport will thus take place only in the thin Ekman layers, which means that q_B will be decreased by another factor $\sim T^{-\frac{1}{2}}$, cf. (3.1c).

Substitution of (3.3) into (2.30a, b) gives, after some algebra,

$$x_0 = x_{0i}; \quad \delta_0 = \delta_{0i} - (t - t_i)\, x_{0i} \tag{3.4a}$$

$$x_1 = x_{1i} - \hat{q}_B(\delta_0) + q_B(\delta_{0i}); \quad \delta_1 = \delta_{1i} - \int_{t_i}^{t} [x_1 + 2\hat{q}_B(\delta_0)]\,\mathrm{d}t, \tag{3.4b}$$

$$x_2 = x_{2i} + \frac{1}{x_{0i}} [\hat{q}_B^2(\delta_0) - \hat{q}_B^2(\delta_{0i})] - \delta_1 \frac{\partial \hat{q}_B}{\partial \delta}(\delta_0) + \delta_{1i} \frac{\delta \hat{q}_B}{\partial \delta}(\delta_{0i}), \tag{3.4c}$$

where δ_{li} and x_{li}, $l = 0, 1, 2$, are prescribed values to zeroth first and second order of δ and x, respectively, for $t = t_i$. The solution depends very sensitively on the accuracy of the approximation of the characteristics. x is therefore computed to $O(\epsilon^2)$ whereas two terms in the series for δ was found to be sufficient. A comparison between (3.4a, b) and a numerical evaluation of (2.30a, b) is shown in table 1. It is unclear whether the series (3.3) are convergent or asymptotic but numerical experiments showed conclusively that the first few terms approximate the exact solution with increasing accuracy for decreasing values of ϵ.

As the buoyancy-driven volume flux of suspension q_B is small, the advection of particles is weak compared with the settling velocity. Coriolis effects will, according to (3.1a), make the advection even weaker. This means that the trajectories of the settling particles are approximately straight lines in the direction of the centrifugal force. Consequently, the characteristics are approximately straight lines that are parallel to the t-axis (cf. 3.4a). The boundary condition (2.31) and the initial condition

(2.32a) at $x = k$ will therefore only influence the solution in the regions $x = 1-O(\epsilon)$ and $x = k+O(\epsilon)$ respectively. The solution (2.30a, b), evaluated in these regions, will consequently make sense only if these regions are significantly larger than the corner regions where the lubrication approximation breaks down, i.e. if $\Lambda^{-\frac{1}{3}} \ll \epsilon$. For $T \sim 1$, this is also a necessary condition for neglecting the slip velocity in (2.24) where it has been assumed that $|u_{Sx}| \ll |u_x^s|$, which is not true if $|u_x^s| \sim \epsilon \sim \Lambda^{-\frac{1}{3}}$. For large values of T, these conditions are different. In the former condition, $\epsilon \sim T^{-\frac{3}{2}}$ leads to $T \ll \Lambda^{\frac{2}{5}}$. The latter condition gives, with $|u_x^s| \sim T^{-1}$,† the less restrictive requirement $T \ll \Lambda^{\frac{1}{3}}$.

In the non-rotating case considered by Herbolzheimer & Acrivos (1981), two shocks appear in the solution. One shock is formed immediately at $x = k$. The other shock is formed in the region $x = 1-O(\epsilon)$ after a finite time. These shocks have to be inserted to remove the non-uniqueness of the solution that appears when characteristics are intersecting. Physical explanations of the mechanisms causing the formation of these shocks were given by Herbolzheimer & Acrivos (1981). Similar shocks will appear also in the case considered in the present work.

If a shock path is denoted by $x = s(t)$ and the notation

$$\delta^{\pm} = \delta(s \pm 0, t)$$

is used, conservation of mass requires that (see e.g. Whitham 1974, p. 30)

$$\dot{s} = \frac{[q(\delta^+)-q(\delta^-)]}{s(\delta^+-\delta^-)} = \frac{s[q_B(\delta^+)-q_B(\delta^-)]}{\delta^+-\delta^-}. \tag{3.5}$$

By far the most common situation in kinematic wave problems is that the characteristics on which $\delta^{\pm}$ are computed are directed into the shock path from each side. If $s(t)$ and $\delta^{\pm}(t)$ are known for $t = \tau$, then $s(\tau+\mathrm{d}\tau)$ can be computed from (3.5). $\delta^{\pm}(\tau+\mathrm{d}\tau)$ can then be computed on the characteristics that cross at $x = s(\tau+\mathrm{d}\tau)$ and the computation can be continued step by step. Unfortunately, s and $\delta^{\pm}$ cannot always be computed by this procedure in the present case since the slope of the characteristics, which is the propagation velocity for wavelets on the interface, is not a monotonic function of δ. The construction of the shock at $x = k$ clearly illustrates the difficulties.

Figure 6(a) shows the triple-valued solution in the neighbourhood of $x = k$ for a small value of t. The characteristic diagram is shown in figure 6(b). There is a fan of intersecting characteristics from $t = 0, x = k$ and a set of characteristics from $t = 0$, $x > k$. The latter characteristics do not intersect each other but intersect those in the fan. The non-uniqueness must be removed by inserting a shock having a path such as that shown in figure 6(b). According to the discussion following (2.32a), the discontinuous variation of δ at $x = k$, which gives rise to the fan, should have no physical effect on the settling and the bulk motion in the channel. It may seem spurious that a discontinuous variation of δ in (2.32a) was then prescribed in the first place. The reason is simply that the formation of a shock at $x = k$ should appear from the mathematical solution of the initial-value problem. If the discontinuity in (2.32a) is deleted, the (unique) solution is determined on the characteristics from $t = 0, x > k$. However, that solution gives $q_B \neq 0$ at $x = k$, which is physically unreasonable. Therefore a shock is constructed where δ^+ is determined on the characteristics that emanate from $t = 0$, $x > k$. However, figure 6(b) shows that there are then no

† This order-of-magnitude relation is not true in regions of geostrophic flow. However, if it holds in the Ekman layers and if $\hat{h} \sim 1$, one can show that the error in the computation of e.g $\delta(x, t)$ is $\sim \Lambda^{-\frac{1}{3}}$.

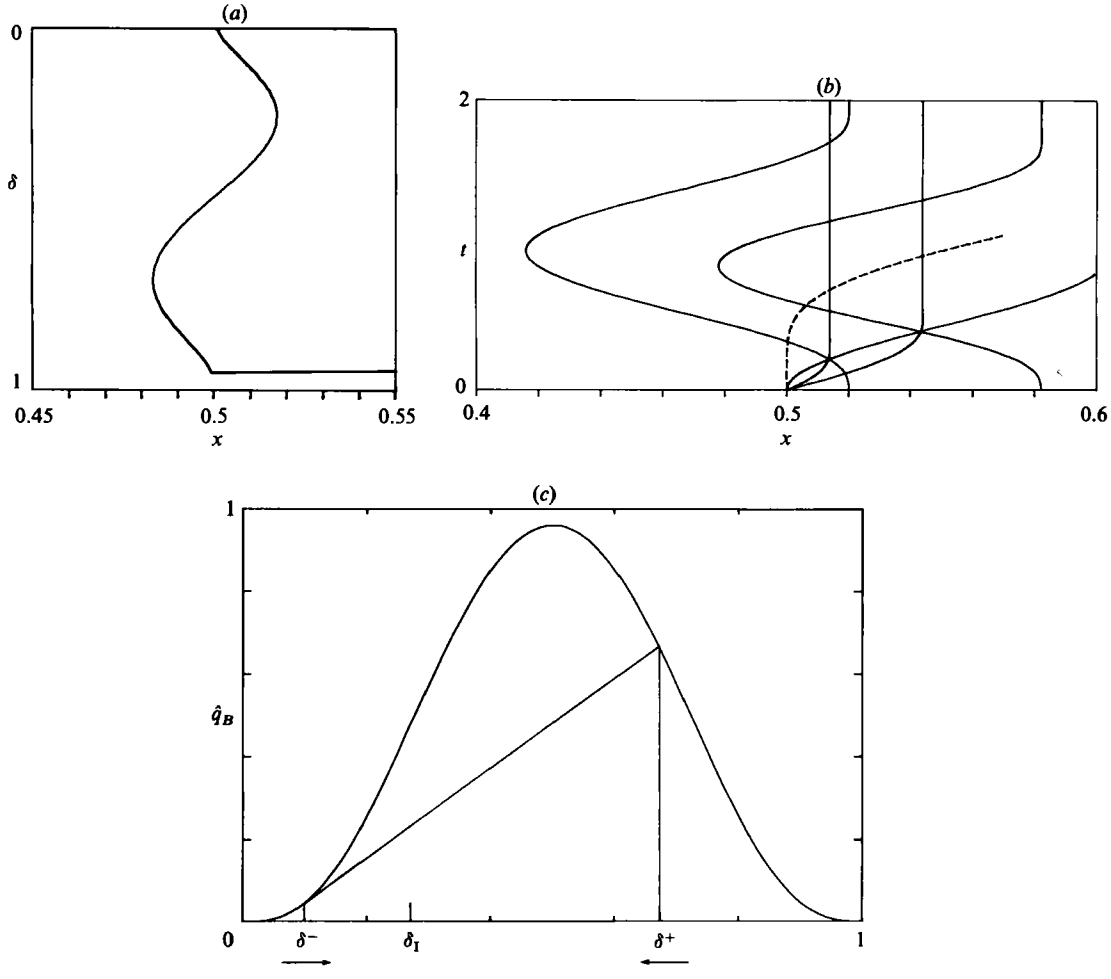

FIGURE 6. (*a*) Multiple-valued solution near $x = k$ for $t = 0.1$ ($k = 0.5$, $T = 4$, $\epsilon = 0.10$). (*b*) Characteristic diagram for the solution in figure 6(*a*): – – –, shock path. (*c*) Shock construction in the $(\hat{q}_B, \delta)$-diagram for the left shock in figure 7. δ_I is the left inflexion point.

characteristics crossing the shock path from the left on which δ^- can be determined. This means that s and $\delta^\pm$ cannot be computed as outlined in the discussion following (3.5). The only way to determine the solution in $k < x < s(t)$ is to construct characteristics that are coming out of the shock path. Unfortunately, unless δ^- is known, there is an infinite number of such constructions.

A very similar situation is encountered in gas dynamics. If the equation of state of the gas is such that the fundamental derivative† can change sign, the same type of difficulty appears. To these author's knowledge, this type of problem was first considered mathematically by Wendroff (1972*a*, *b*). In scalar hyperbolic problems of first order, Wendroff showed that characteristics that are coming out of a shock path must do so tangentially. This condition is also implicit (cf. (2.18)) in the work by Lax (1973) and in the treatise by Jeffrey (1976, p. 154). In a recent paper, Cramer & Kluwick (1984) gave a number of illuminating explicit solutions for weak gas-dynamic

† This quantity is defined as $\partial(a\rho)/\partial\rho$, where a is the speed of sound and ρ is the density.

shocks and also showed that these solutions can be regarded as limits of solutions of a more realistic problem with diffusive effects included (cf. 2.33). In the present problem, Wendroff's condition means that according to (2.26) and (2.29*b*) one must impose

$$\dot{s} = s\,\frac{\partial q_{\mathrm{B}}}{\partial \delta}\,(\delta^-) \tag{3.6}$$

for the shock at $x = k$. If $s(\tau)$ and $\delta^+(\tau)$ are known, $s(\tau+\mathrm{d}\tau)$ and $\delta^+(\tau+\mathrm{d}\tau)$ can be computed by the procedure outlined in the discussion following (3.5) whereas $\delta^-(\tau+\mathrm{d}\tau)$ is computed by eliminating $\dot{s}$ between (3.5) and (3.6). The shock at $x = k$ computed by Herbolzheimer & Acrivos (1981) does not fulfil (3.6).

In the present context, it may be of interest to point out that a shock construction of this kind is, in some cases, necessary for the computation of the clear fluid–suspension interface in batch settling in a rotating container, whose aspect ratio is of order unity (Anestis & Schneider 1983).

If s is assumed to possess an expansion of the form (3.3) one obtains from (3.5) and (3.6), after some algebra, the following set of equations:

$$\dot{s}_0 = 0 \quad (s_0(0) = k), \tag{3.7a}$$

$$\dot{s}_1 = \frac{s_0[\hat{q}_{\mathrm{B}}(\delta_0^+) - \hat{q}_{\mathrm{B}}(\delta_0^-)]}{\delta_0^+ - \delta_0^-} = s_0\,\frac{\partial \hat{q}_{\mathrm{B}}}{\partial \delta}\,(\delta_0^-) \quad (s_1(0) = 0), \tag{3.7b}$$

$$\dot{s}_2 = s_1\,\frac{\partial \hat{q}_{\mathrm{B}}}{\partial \delta}\,(\delta_0^-) + \delta_1^-\,s_0\,\frac{\partial^2 \hat{q}_{\mathrm{B}}}{\partial \delta^2}\,(\delta_0^-) \quad (s_2(0) = 0), \tag{3.7c}$$

$$\frac{\delta_1^+\left[\dfrac{\partial \hat{q}_{\mathrm{B}}}{\partial \delta}\,(\delta_0^+) - \dfrac{\partial \hat{q}_{\mathrm{B}}}{\partial \delta}\,(\delta_0^-)\right]}{\delta_0^+ - \delta_0^-} = \delta_1^-\,\frac{\partial^2 \hat{q}_{\mathrm{B}}}{\partial \delta^2}\,(\delta_0^-). \tag{3.7d}$$

Using the solution (3.4*a*, *b*), this system is readily integrated numerically as indicated in the discussion following (3.2) and (3.6). For $T = 0$ and small values of t, one can find an approximate solution which may serve to illustrate the structure of the solution near $x = k$. The position of the shock and the location of the interface on each side of it are given by the expressions

$$s = k + \epsilon(t^4 - \tfrac{4}{5}t^5) + \ldots, \tag{3.8a}$$

$$\delta^+ = 1 - kt - 80\epsilon k^3 t^4 + \ldots, \tag{3.8b}$$

$$\delta^- = \tfrac{\sqrt{6}}{12}(t^{\frac{3}{2}} - \tfrac{1}{2}t^{\frac{5}{2}} + \ldots). \tag{3.8c}$$

There is a region $0 < y < 1$, $k < x < x_{\mathrm{c}}(t)$, say, where the suspension has settled completely. The approximate expression for $x_{\mathrm{c}}(t)$ is

$$x_{\mathrm{c}} = k + \epsilon\,(t^4 - \tfrac{4\sqrt{6}}{9}\,t^{\frac{9}{2}} + \ldots). \tag{3.8d}$$

The construction of the shock in the $(\hat{q}_{\mathrm{B}}, \delta)$-diagram is shown in figure 6(*c*). According to (3.5) and (3.6), the secant is tangential to the curve $\hat{q}_{\mathrm{B}}(\delta)$ at $\delta = \delta^-$. The shock strength decays to zero in a finite time as $\delta^{\pm}$ monotonically approach the left inflexion point at $\delta = \delta_{\mathrm{I}}$. It can be shown that during the final state of decay

$$\delta^- = -\tfrac{1}{2}\delta^+ + \tfrac{3}{2}\delta_{\mathrm{I}} + O(|\delta^+ - \delta^-|^2). \tag{3.9}$$

This relation is general and holds for any value of T.

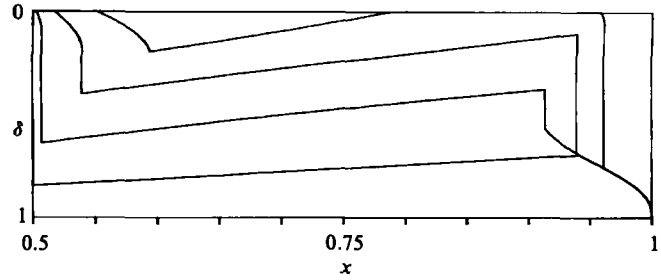

FIGURE 7. Location of the interface in batch settling for $t = 0.3, 0.6, 0.9, 1.2$ ($k = 0.5$, $T = 4$, $\epsilon = 0.10$).

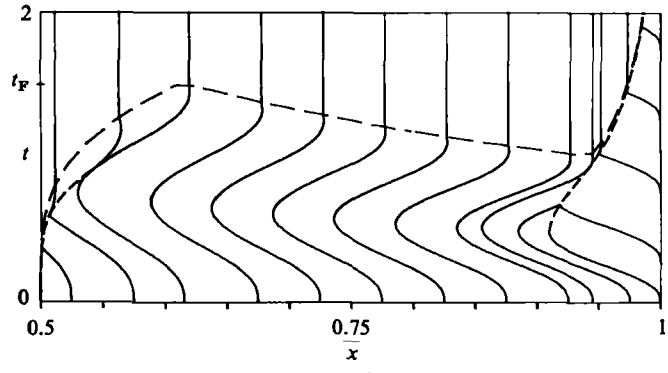

FIGURE 8. Characteristic diagram for the solution shown in figure 7: – – –, shock path; — —, contact line $x_c(t)$ were $\delta(x_c, t) = 0$. The suspension outside the end region $x = 1 - O(\epsilon)$ has settled for $t = t_F$.

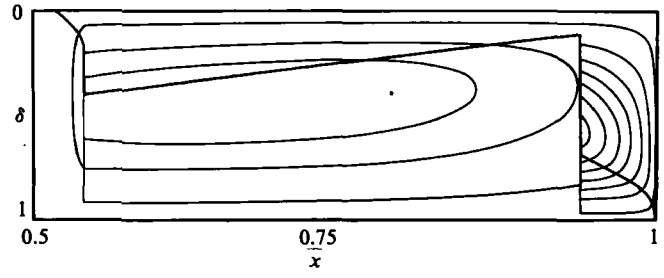

FIGURE 9. Streamlines for the solution in figure 7 at $t = 0.9$. The values of the stream function are $\Psi = 0.00001 + n \times 0.00005$, $n = 1, 2 \ldots 6$: ——, streamlines; ——, location of the interface.

Figure 7 shows the solution $\delta(x, t)$ for $T = 4$. Shock paths, characteristics and the location of the contact line $x_c(t)$ are shown in figure 8. For this value of T, the velocity field is practically unaffected by the Coriolis force. The only noticeable effect of rotation is the x-dependent settling velocity.

It can be seen from the characteristic diagram in figure 8 that the shock in the region $x = 1 - O(\epsilon)$ is, during most of the time, of conventional type, i.e. with characteristics that are directed into the shock from both sides. As in the non-rotating case, this shock appears after a finite time and, because $\delta(t)$ is the same along the characteristics from $x = 1$, $t > 0$, the interface in the region $s(t) < x < 1$ is steady. The shock

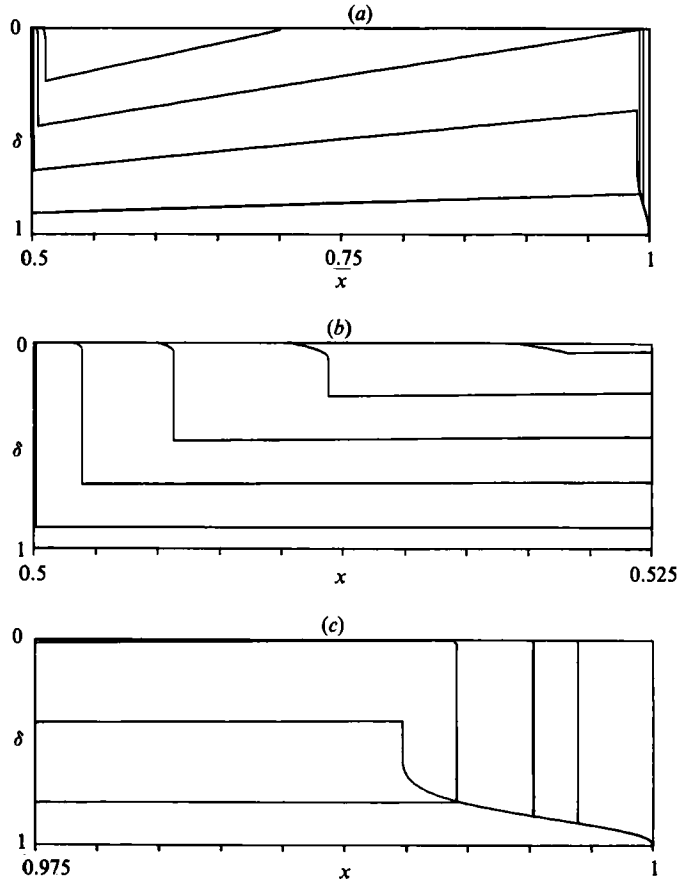

FIGURE 10. (*a*) Location of the interface in batch settling for $t = 0.2, 0.6, 1.0, 1.4$ ($k = 0.5$, $T = 64$, $\epsilon = 0.0103$). (*b*) Enlarged view of the left end of figure 10(*a*) for $t = 0.2, 0.6, 1.0, 1.4, 1.8$. (*c*) Enlarged view of the right end of figure 10(*a*) for $t = 0.2, 0.6, 1.0, 1.4, 1.8$.

approaches asymptotically the closed end at $x = 1$ for large values of t according to the formulas

$$s = 1-\epsilon\mu^3 A^3 \mathrm{e}^{-2t}+\ldots, \quad \delta^+ = 1-\tfrac{1}{4}\mu A \mathrm{e}^{-\frac{2}{3}t}+\ldots, \quad \delta^- = \frac{\mu^{\frac{3}{2}}A^{\frac{3}{2}}}{4\sqrt{6}}\mathrm{e}^{-t}+\ldots, \quad (3.10)$$

where $\mu \ll 1$ is a measure of the deviation from the final state and the constant $A \sim 1$ is determined from the full solution. (3.10) does not mean that, in reality, the suspension never settles completely but is merely a consequence of the failure of the lubrication approximation to correctly represent the flow in the corner regions. If the small amount of suspension in $s < x < 1$ is disregarded, an appropriate measure of the time for complete settling, $t = t_{\mathrm{F}}$, say, is the time required to clarify the suspension in the rest of the channel, $k < x < s$ (see figure 8).

Some distance away from the end regions (see figure 7) the interface attains approximately the shape of a cone. Because the settling velocity increases linearly with x, the angle of this cone is larger than that of the disks. The slight deviation from a conical shape is caused by the weak buoyancy-driven advection of particles.

Figure 9 shows some streamlines for the case shown in figure 7. Apart from the discontinuities across the two shocks, the streamlines are, as expected, closed.

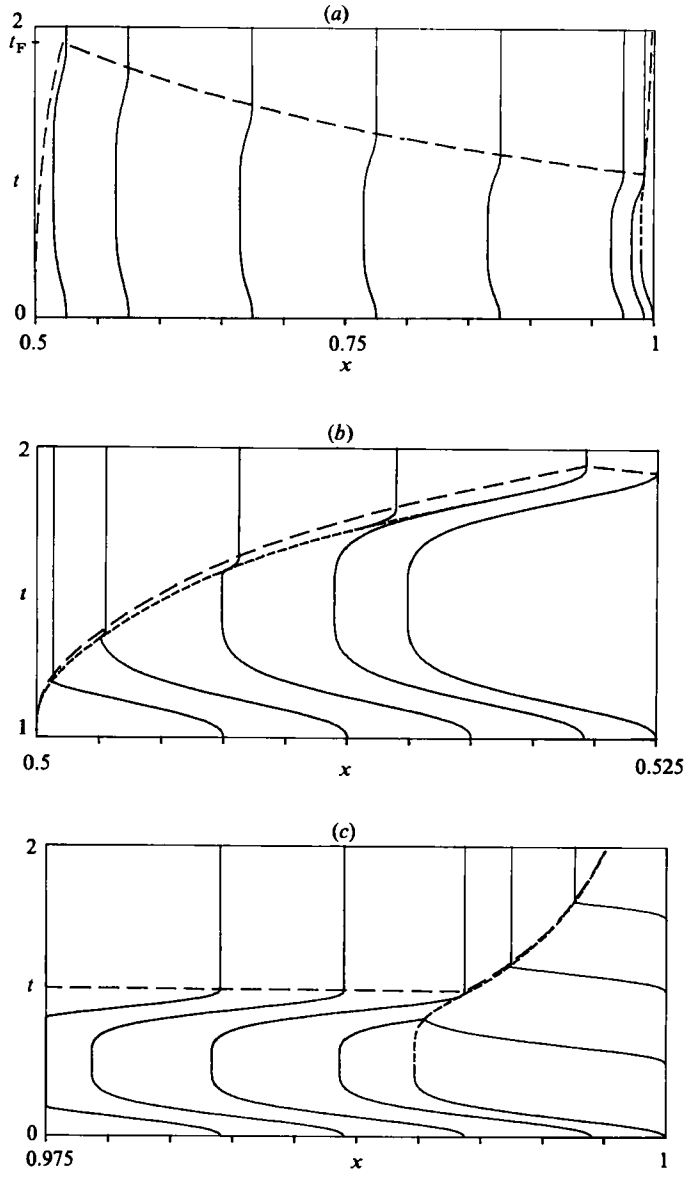

FIGURE 11. (*a*) Characteristic diagram for the solution shown in figure 10 (*a*). – – –, shock path; — —, contact line $\delta(x,t) = 0$, the shock paths in the end regions practically coincide with this curve. t_F is the time when all suspension outside the right end region $x = 1-O(\epsilon)$ has settled. (*b*) Enlarged view of the left end of figure 11 (*a*). (*c*) Enlarged view of the right end of figure 11 (*a*).

The location of the interface in a case with significant Coriolis effects on the velocity field, cf. figure 3, is shown in figure 10 (*a–c*). Figure 10 (*b, c*) are enlarged versions of figure 10 (*a*) in the end regions. The geometry of the channel is the same as in the previous case. The corresponding characteristic diagrams are shown in figure 11 (*a–c*). As was pointed out in the discussion preceding (3.4*a, b*), a larger value of T implies a smaller value of ϵ. This means that the regions where effects of the closed ends of the channel are felt are smaller than in the case shown in figure 7. Also, equivalently,

the deviation of the characteristics from straight lines that are parallel with the t-axis is smaller in figure 11 (a) than in figure 8.

It can be seen from figures 11 (a) and 8 that the dimensionless time t_F for complete settling is somewhat larger in the rapidly rotating case. The reason is the following: because $\delta = 0$ in some neighbourhood of $x = k$ and the settling is more rapid for larger values of x, there will be a maximum value of $\delta = \delta_m$ near the inner end, see figures 7 and 10 (a). (An equivalent definition of t_F is that $\delta_m(t_F) = 0$.) The volume of suspension between $y = 0$ and $y = \delta_m$ tends to be pushed toward larger values of x by the centrifugal force, i.e. into a region where the settling is faster. However, this motion is retarded by the Coriolis force. Thus, for larger values of T, the main part of the suspension tends to remain in a region where the settling is relatively slow. However, this effect is much more than compensated for if one considers the dimensional values t_F^*. For two identical channels that are rotating with the angular velocities Ω_1 and Ω_2, with the corresponding Taylor numbers T_1 and T_2 respectively, one finds from (2.5), (2.6) and (2.9) that

$$\frac{t_{F1}^*}{t_{F2}^*} = \frac{T_2^2 t_{F1}}{T_1^2 t_{F2}}. \tag{3.11}$$

4. The filling problem ($Q < 0$)

When a suspension of heavy particles in a light liquid is separated in a continuously operating centrifuge, the suspension is, in many designs, fed into the disk stack at its outer end. There are more-complicated designs where the flow is non-axisymmetric (see e.g. Sokolov 1971) but these will not be considered in this work. Under certain conditions, the fluid that leaves the disk stack at the inner end will be clarified and sediment will come out from the stack at the outer end. For a maximum throughput with complete separation, the particles that enter a channel near the inner disk should settle on the outer disk near the outlet. This section deals with how such a process may be set up in an idealized case where a suspension of constant concentration is pumped into a channel that initially contains clear fluid.

Because the suspending fluid is required to carry the particles a (non-dimensional) distance of order unity into the channel, the velocity component in the x-direction must be of order unity. The total volume flux $Q < 0$ must consequently be such that $|Q| \sim 1$. According to (2.26) and (3.2), the total volume flux of suspension can be written

$$q = \epsilon x^2 \hat{q}_B(\delta) + Q q_Q(\delta). \tag{4.1}$$

As the only cases where $\epsilon \ll 1$ are considered in this work, the dynamical effect of the difference in density between suspension and clear fluid can, on reasonable grounds, be expected to be small. It can be shown that this may not be so in regions where $\partial\delta/\partial x$ is very large, i.e. regions that in the present work are modelled as shocks. Inside such regions, buoyancy is, in certain cases, important even if $\epsilon \ll 1$ and $|Q| \sim 1$. Details of this matter will be reported elsewhere. The function $q_Q(\delta)$ is shown in figure 12 for some values of T.

If expansions of the form (3.3) are assumed for δ and x, the lowest-order solution obtained from (2.30a, b) is

$$x = \{x_{0i}^3 + 3Q[q_Q(\delta_{0i}) - q_Q(\delta_0)]\}^{\frac{1}{3}}, \tag{4.2a}$$

$$t_i - t = \int_{\delta_{0i}}^{\delta_0} \frac{\mathrm{d}\delta'}{x_0(\delta')}. \tag{4.2b}$$

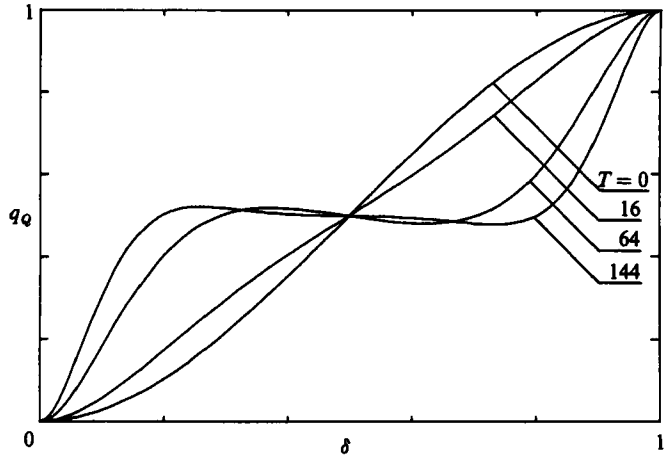

FIGURE 12. The function $q_Q(\delta)$ for some values of T.

δ	exact t	approx. t	exact x	approx. x
0.99	0.0100	0.0100	0.9983	0.9983
0.75	0.2762	0.2756	0.8476	0.8477
0.50	0.5579	0.5574	0.8548	0.8549
0.25	0.8609	0.8605	0.8620	0.8621
0.00	1.1836	1.1818	0.6300	0.6300

TABLE 2. Numerical comparison between (2.30a, b) and (4.2a, b) for $k = 0.5$, $T = 144$, $\epsilon = 0.00302$, $Q = -0.25$. In contrast to table 1, δ is here taken as the independent variable. This leads to somewhat simpler computations because both (2.22b) and (4.2b) are integrals with respect to δ.

This approximate solution describes a situation where the particles are falling passively in the suspending fluid.† The higher-order corrections are considerably more complicated than in the batch-settling case. For simplicity attention will therefore henceforth be restricted to cases where ϵ is very small and (4.2a, b) can be used with accuracy. The subscript 0 will be deleted in what follows. A numerical comparison between (4.2a, b) and the exact solution is shown in table 2.

As a preliminary, a simple case with negligible effects of rotation on the velocity field, i.e. $T \ll 1$, will be considered. ϵ can be made sufficiently small by choosing a small value of h (see 3.1b). The expression for q_Q with $T = 0$ is given in the Appendix. The behaviour of the solution for small times, which is most conveniently obtained directly from (2.29a, b), is given by

$$\delta = \delta_i - t + O(t^2) \quad (0 < \delta_i < 1), \tag{4.3a}$$

$$x = 1 + u_x^s(\delta_i)\, t + O(t^2), \tag{4.3b}$$

where

$$u_x^s(\delta) = \frac{Q}{x}\frac{\partial q_Q}{\partial \delta} = \frac{6Q}{x}\delta(1-\delta) \tag{4.3c, d}$$

† An interesting property of this solution is that the characteristics are the trajectories in the (x, t)-plane of the particles at the interface. This follows from (2.25), (2.29b) and the fact that the bulk velocity field is independent of δ.

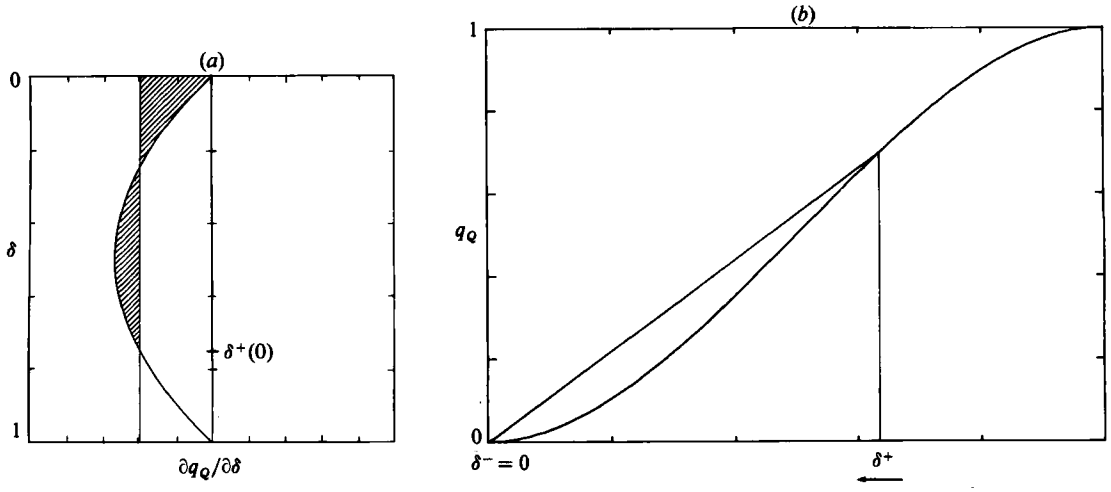

FIGURE 13. (*a*) Equal-area construction applied to the flux function q_Q to determine $\delta^+(0)$ for the case in figure 14(*a*). (*b*) Shock construction in the (q_Q, δ)-diagram for the solution shown in figure 14(*a*).

is the velocity in the x-direction, normalized according to (2.27*a*, *b*), of the particles at the interface. Elimination of δ_i in (4.3*a*, *b*) gives

$$x = 1 + u_x^s(\delta)\, t + O(t^2) \quad (0 < \delta < 1), \tag{4.4}$$

which simply means that, for small times, the multivalued solution $\delta(x, t)$ has the same form as the parabolic velocity profile. A shock will thus appear immediately and the computation of $s(t)$ and $\delta^{\pm}(t)$ requires specification of $\delta^{\pm}(0)$. To obtain a single-valued solution, one must obviously take $\delta^-(0) = 0$ because the particles on the interface near $y = 0$ are advected in the x-direction with a vanishing velocity. $\delta^+(0)$ is determined from the equal-area rule (Whitham 1974, p. 42), which means that the shock must be constructed in such a way that the volume of suspension is conserved. The construction is illustrated in figure 13(*a*). One obtains from this figure

$$\delta^+ u_x^s(\delta^+) = \frac{Q}{s}\, q_Q(\delta^+), \tag{4.5}$$

$$\dot{s} = \frac{Q}{s}\,\frac{q_Q(\delta^+)}{\delta^+} = \frac{Q}{s}\,\frac{\partial q_Q}{\partial \delta}\,(\delta^+), \tag{4.6}$$

which means that in the shock construction in the (q_Q, δ)-diagram, see figure 13(*b*), the secant is initially tangential to the curve $q_Q(\delta)$. This result is independent of the particular form of $q_Q(\delta)$ and will be used later in this section. For the form given by (4.3*d*), $\delta^+(0+) = \frac{3}{4}$. It can be shown that the equal-area rule is, for several reasons, only applicable in the present problem for small times. One reason is that the volume of suspension is not conserved for finite times but is approximately conserved for small times. Further aspects of this matter is discussed in the Appendix of the paper by Cramer & Kluwick (1984).

The characteristic diagram is shown in figure 14(*b*). The initial discontinuity in δ gives a fan of intersecting characteristics from $x = 1$, $t = 0$. The non-uniqueness is removed by insertion of a shock as described in the previous paragraph and thereby only non-intersecting characteristics will be left in the fan. Ahead of the shock, i.e. in $x < s(t)$, $\delta = 0$ and the characteristics are parallel with the t-axis. As can be seen

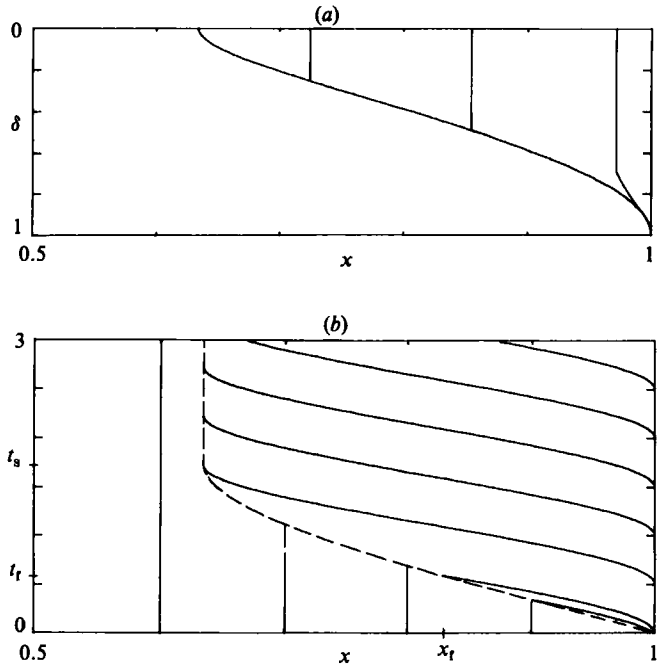

FIGURE 14. (*a*) Location of the interface in the filling problem for $t = 0.1, 0.5, 1.0, 2.0$ ($k = 0.5, T = 0$, $\epsilon = 0$, $Q = -0.25$). The interface is initially unsteady in $s < x < 1$ but later becomes steady. (*b*) Characteristic diagram for the solution shown in figure 14(*a*): – – –, shock path. The solution in $x_f \leqslant x \leqslant 1$, $0 \leqslant t \leqslant t_f$ is determined by the fan from $x = 1$, $t = 0$. The final steady shape of the interface is reached when $t \leqslant t_s$.

from figure 14(*b*), the characteristics are in this case directed into the shock path from both sides. The shock path is thus computed by numerical integration of the left part of (3.5) with $q = Qq_Q$. In addition to the characteristics in the fan, there are also characteristics from $x = 1$, $t > 0$ behind the shock. Along these characteristics, which have the same shape, $\delta(t)$ is the same. This means that after the first characteristic with $\delta_i = 1$, $x_i = 1$ has reached the shock path at $x = x_f$, $t = t_f$, say, see figure 14(*b*), the shape of the interface in $s(t) < x < 1$ will be steady. For obvious reasons, the strength of the shock decays monotonically to zero. These properties of the solution are clearly illustrated in figure 14(*a*), which shows $\delta(x, t)$.

It is of interest to investigate how the steady state with $\delta^+ = 0$ is approached. From (4.2*a*) one finds that the final shape of the interface is given by

$$x = \{1 + 3Q[1 - (3\delta^2 - 2\delta^3)]\}^{\frac{1}{3}}. \tag{4.7}$$

If one writes

$$\delta^+(t) = \mu\Delta(t) + O(\mu^2), s(t) = (1+3Q)^{\frac{1}{3}} + \gamma(\mu)\, S(t) + o(\gamma), \tag{4.8}$$

where it has been assumed that μ, γ are $o(1)$ and Δ and S are $O(1)$, one finds, after some algebra, from (4.6) that

$$\gamma = \mu^2, \quad S = \left[\frac{3Q(t_s - t)}{2\mu}\right]^2, \quad \Delta = (1+3Q)^{\frac{1}{3}} (S/|Q|)^{\frac{1}{2}}. \tag{4.9}$$

Here t_s is the *finite* time at which the steady state is reached. t_s can only be determined from the complete solution. (4.9) has been derived under the assumption that the

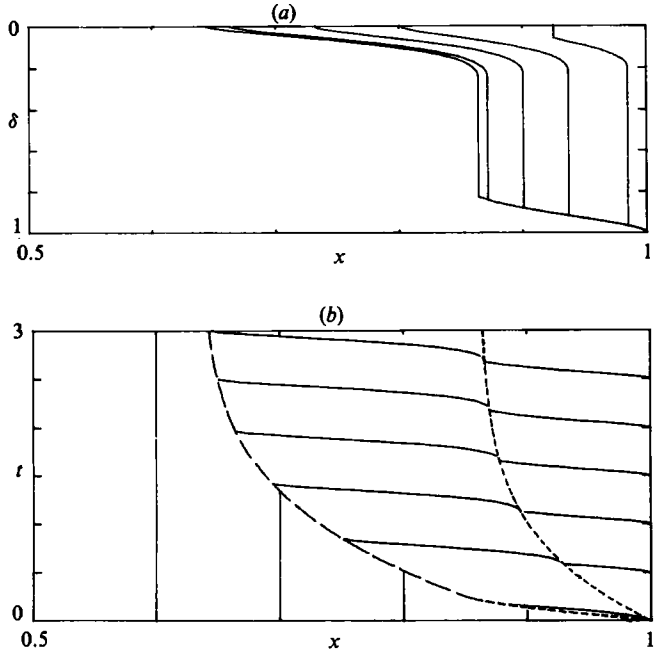

FIGURE 15. (*a*) Location of the interface in the filling problem for $t = 0.1$, 0.5, 1, 2, 3 ($k = 0.5$, $T = 144$, $\epsilon = 0.00302$, $Q = -0.25$). (*b*) Characteristic diagram for the solution shown in figure 16(*a*): – – –, shock path: — —, contact line $\delta(x,t) = 0$.

shock strength decays to zero for $t > t_f$. Cases where this condition is not fulfilled, i.e. short channels, seem to be of less practical importance and are not considered here.

A quantity of practical interest is the maximum throughput $|Q|_{\max}$ with complete separation (in the steady state) for a given location of the inner edge of the disks ($x = k$). (4.2*a*) with $q(\delta_i) = Q_{\max}$ and $q(k) = 0$ gives

$$|Q|_{\max} = \frac{1-k^3}{3}. \tag{4.10}$$

This result, which is valid for any value of T, seems to have been first given by Svarovsky (1971) for $T \ll 1$. It should be noted that the shape of the interface varies with T. In dimensional terms, (4.10) means that $Q^*_{\max}$, for a given geometry of the channel, increases with the square of the angular velocity of the channel.

The solution for $T = 144$ is shown in figure 15(*a*). Two shocks will appear in this case. The location of these shocks are denoted by $x = s_l(t)$ and $x = s_u(t)$, respectively, where the subscripts imply lower and upper ($s_u < s_l$). Figure 16(*a*) shows the equal-area construction for computing $\delta_l^{\pm}(0)$ and $\delta_u^{\pm}(0)$. The shock construction in the (q_Q, δ)-diagram is shown in figure 16(*b*). Characteristics and shock paths are shown in figure 15(*b*).

The upper shock has a similar character to that in the previous case whereas the nature of the lower shock is different. In the same way as in the previous case, the equal-area construction, see figure 15(*a*), leads to (4.6) for the upper shock and the following relation for the lower shock:

$$\dot{s}_l = \frac{Q[q_Q(\delta_l^+) - q_Q(\delta_l^-)]}{s_l(\delta_l^+ - \delta_l^-)} = \frac{Q}{s_l}\frac{\partial q_Q}{\partial \delta}(\delta_l^+) \quad (t = 0+). \tag{4.11}$$

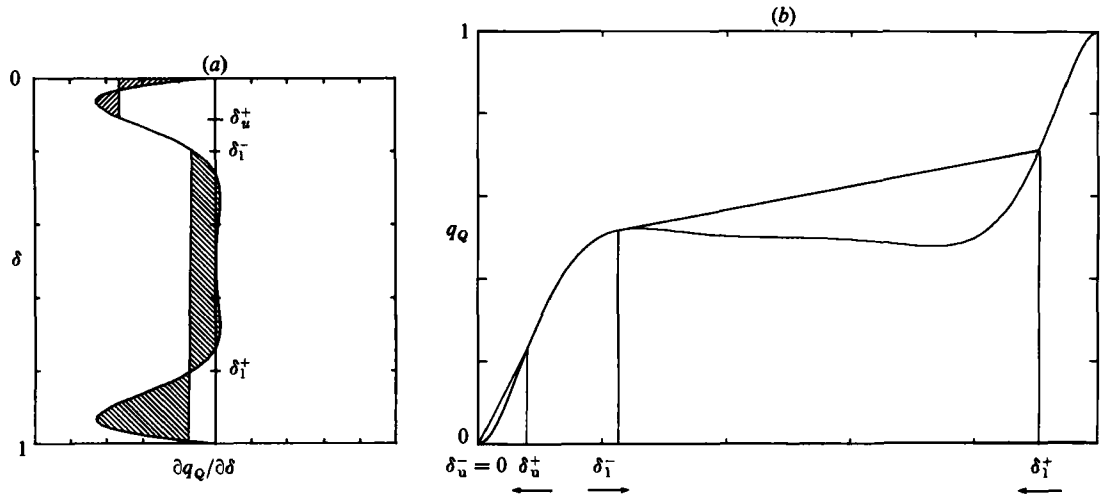

FIGURE 16. (*a*) Equal-area construction applied to the flux function q_Q to determine $\delta_1^{\pm}(0)$ and $\delta_u^+(0)$ for the case shown in figure 15(*a*). (*b*) Shock construction in the (q_Q, δ)-diagram for the solution shown in figure 15(*a*).

Because the characteristics are the trajectories in the (x, t)-plane of the particles at the interface and the particles are advected in the negative x-direction,† see the velocity profiles in figure 4, characteristics must come out from the lower shock into the region $x < s_1(t)$. As was discussed in some detail in the previous section, one must therefore require that (cf. (3.6))

$$\dot{s}_1 = \frac{Q}{s_1}\frac{\partial q_Q}{\partial \delta}(\delta_1^-) \quad (t > 0). \tag{4.12}$$

The path of the lower shock is thus computed from the left-hand part of (3.5) with $q = Qq_Q$ and (4.12) by using the procedure outlined after (3.6). The strength of this shock does not decay to zero as the steady state is approached. The asymptotic values $\delta^{\pm}(\infty)$ are readily determined geometrically from the curve in figure 15(*b*) by drawing the horizontal secant between δ_1^+ and δ_1^-, with δ_1^- such that (4.12) is fulfilled. When $\delta_1^+(\infty)$ is known, the steady shape of the interface in $s_1(\infty) < x < 1$ can be computed from (4.2*a*) as in the previously discussed case for $T \ll 1$.

The approach of the lower shock to the steady state can be computed by using standard regular perturbation methods. Assuming expansions of the form (cf. (4.8))

$$\left.\begin{aligned} &\delta_1^+(t) = \delta_\lambda^+(\infty) + \mu\Delta(t), \quad \delta_1^-(t) = \delta_1^-(\infty) + O(\mu^2), \\ &s_1(t) = s_1(\infty) + \gamma(\mu)\,S(t) + o(\gamma), \end{aligned}\right\} \tag{4.13}$$

one finds

$$\gamma = \mu, \quad \Delta = \frac{s_1^2(\infty)\,S(t)}{Q\dfrac{\partial q_Q}{\partial\delta}(\delta_1^+(\infty))}, \quad S(t) = A\exp\left[-\frac{s_1(\infty)\,t}{(\delta_1^+(\infty) - \delta_1^-(\infty))}\right], \tag{4.14}$$

where A is a constant that must be determined from the complete solution.

The general character of the solution in $s_u(t) < x < s_1(t)$ is very similar to the

† This is not true in the small regions of backflow in the Ekman layers. However, it can be shown that this does not affect the argument.

solution in the previously discussed case for small values of T. The main difference is that, for finite values of T, the quantities $x_i = s_1(t)$ and $\delta_i = \delta_1^-(t)$, which determine the solution on the characteristics, are not constants. The location of the interface between the two shocks is therefore time-dependent. For the case shown in figure 16, the strength of the upper shock decays quite rapidly to zero and is replaced by a moving contact line (see e.g. figure 16a). When the lower shock is close to its asymptotic position, the shape of the interface in $x < s_1(t)$ can be computed approximately from (4.2a) with $\delta_{0i} = \delta_1^-(t)$.

Although the previous discussion in mathematical terms is rather involved, the results can be interpreted in a simple, albeit qualitative, way by considering the motion of passively falling particles in a velocity field of the kind that is shown in figure 4. The particles entering the channel in the Ekman layer at $y = 1$ will fall out from this layer into the region of geostrophic flow where the velocity in the x-direction is negligible. Because the velocity profile is non-monotonic, the interface between clear fluid and suspension will immediately fold over itself and the lower shock is formed. For the same reason, the upper shock will be formed in the Ekman layer at $y = 0$. The particles that are falling in the geostrophic region behind the lower shock will be accelerated when they enter the Ekman layer at $y = 0$. The upper shock will therefore propagate faster into the channel than the lower one. Because there are two maxima in the velocity profile, the strength of the lower shock will be finite also when the steady state is attained. One finds that the lower shock occurs for $T > 39.5$.

Finally, it should be pointed out that it follows directly from (4.2a) and (4.11) with $\dot{s}_1 = 0$ that (4.10) is valid even if there is a shock in the steady state.

5. Conclusions

The theoretical results by Herbolzheimer & Acrivos (1981) for time-dependent settling of a dilute monodisperse suspension due to gravity in narrow tilted channels have been extended to axisymmetric settling in the centrifugal field between two narrowly spaced and rapidly rotating conical disks. Two problems have been solved: batch settling, and the problem where a suspension is pumped from the outer end into a channel that is initially filled with clear fluid. The main results are:

Batch settling

The general character of the solution is similar to that in the plane, non-rotating case studied by Herbolzheimer & Acrivos (1981). It is shown that the shock construction given in that work must be partly modified according to the results of Wendroff (1972a, b).

The buoyancy-driven motion of clear fluid and suspension, which can be characterized as long gravity waves of finite amplitude at low Reynolds number, tends to be blocked by rotation. For large Taylor numbers, i.e. when Coriolis effects are strong, meridional flow will take place only in the Ekman layers. This flow is considerably weaker than the flow at small Taylor numbers.

Filling problem

For small values of the Taylor number, one shock appears in the solution. The strength of this shock decays to zero. For large Taylor numbers there are two shocks. One of these decays with time whereas the other one remains of finite strength for all times. The steady state is reached after a finite time for small Taylor numbers but approached exponentially for large Taylor numbers. In spite of the very different

character of the steady solution for small and large Taylor numbers, the same simple formula for the maximum throughput is valid for all Taylor numbers.

This work has been partially supported by the Swedish Board for Technical Development (STU) and Alfa Laval AB.

Appendix. The functions $q_B(\delta)$ and $q_Q(\delta)$

In terms of the variables

$$\eta = 1-2\delta, \quad \mu = \tfrac{1}{2}T^{\frac{1}{2}}$$

the functions q_B and q_Q can be written

$$q_B = 2\pi\hat{h}^3 \sin^3\alpha \frac{A+B}{128\mu^3 a}, \quad q_Q = \frac{1}{2}-\frac{h}{c},$$

where

$$A = c\left[1-\left(\frac{2h}{c}\right)^2\right], \quad B = \frac{ed^+ + fd^-}{b},$$

$$a(\mu) = \cosh^2\mu\cos^2\mu + \sinh^2\mu\sin^2\mu,$$

$$b(\mu) = \sinh^2\mu\cos^2\mu + \cosh^2\mu\sin^2\mu,$$

$$c(\mu) = \sinh 2\mu - \sin 2\mu,$$

$$d^{\pm}(\mu) = \sinh 2\mu(1-2\sin^2\mu) \pm \sin 2\mu(1+2\sinh^2\mu)$$

$$e(\eta,\mu) = (1-\cosh[\mu(\eta-1)]\cos[\mu(\eta-1)])(1-\cosh[\mu(\eta+1)]\cos[\mu(\eta+1)])$$
$$-\sinh[\mu(\eta-1)]\sin[\mu(\eta-1)]\sinh[\mu(\eta+1)]\sin[\mu(\eta+1)],$$

$$f(\eta,\mu) = \sinh[\mu(\eta-1)]\sin[\mu(\eta-1)](1-\cosh[\mu(\eta+1)]\cos[\mu(\eta+1)])$$
$$+\sinh[\mu(\eta+1)]\sin[\mu(\eta+1)](1-\cosh[\mu(\eta-1)]\cos[\mu(\eta-1)]),$$

$$h(\eta,\mu) = \sinh(\mu\eta)\cos(\mu\eta)\cosh\mu\cos\mu + \cosh(\mu\eta)\sin(\mu\eta)\sinh\mu\sin\mu$$
$$+\sinh(\mu\eta)\cos(\mu\eta)\sinh\mu\sin\mu - \cosh(\mu\eta)\sin(\mu\eta)\cosh\mu\cos\mu.$$

For $T = 0$

$$q_B(T=0) = 2\pi\hat{h}^3\sin^3\alpha\frac{\delta^3(1-\delta)^3}{3},$$

$$q_Q(T=0) = \delta^2(3-2\delta).$$

Note added in proof: Recently two papers dealing with similar problems as in this work but for $\hat{h} \sim \Lambda^{\frac{1}{3}}$ have appeared in the literature; Greenspan 1985(*a*, *b*).

REFERENCES

Acrivos, A. & Herbolzheimer, H. 1979 *J. Fluid Mech.* **92**, 435.

Anestis, G. & Schneider, W. 1983 *Ingenieur-Archiv* **83**, 399.

Bark, F. H., Johansson, A. V. & Carlsson, C. G. 1984 *J. Méc. Théorique et Appliquée* **3**, 861.

Barnea, E. & Mizrahi, J. 1973 *Chem. Engng J.* **5**, 171.

BATCHELOR, G. K. 1967 *An Introduction to Fluid Dynamics*. Cambridge University Press.

BOYCOTT, A. E. 1920 *Nature* **104**, 532.

CHAN, D. & POWELL, R. L. 1984 *J. Non-Newtonian Fluid Mech.* **15**, 165.

CRAMER, M. S. & KLUWICK, A. 1984 *J. Fluid Mech.* **142**, 9.

DAVIS, R. H., HERBOLZHEIMER, E. & ACRIVOS, A. 1982 *Intl J. Multiphase Flow* **8**, 571.

DIPRIMA, R. C. 1969 *J. Lubrication Tech.* **91**, 45.

DREW, D. A. 1983 *Ann. Rev. Fluid Mech.* **15**, 261.

ENGQUIST, B. & OSHER, S. 1981 *Math. Comp.* **36**, 125.

GREENSPAN, H. P. 1968 *The Theory of Rotating Fluids*. Cambridge University Press.

GREENSPAN, H. P. 1983 *J. Fluid Mech.* **127**, 91.

GREENSPAN, H. P. 1985*a* *J. Fluid Mech.* **157**, 359.

GREENSPAN, H. P. 1985*b* *Intl J. Multiphase Flow* **11**, 825.

HERBOLZHEIMER, E. & ACRIVOS, A. 1981 *J. Fluid Mech.* **108**, 485.

HSU, H.-W. 1981 *Separation by Centrifugal Phenomena*. Wiley.

ISHII, M. 1975 *Thermo-fluid Dynamic Theory of Two-phase Flow*. Eyrolles.

JEFFREY, A. 1976 *Quasilinear Hyperbolic Systems and Waves*. Pitman.

KLUWICK, A. 1977 *Acta Mech.* **26**, 15.

KYNCH, G. J. 1952 *Trans. Faraday Soc.* **48**, 166.

LAX, P. D. 1973 *SIAM Regional Conf. Series, in Appl. Math. No.* 11 (1973).

LEUNG, W.-F. & PROBSTEIN, R. F. 1983 *I & EC Process Design & Development* **22**, 58.

LIGHTHILL, M. J. & WHITHAM, G. B. 1955 *Proc. R. Soc. Lond.* A **299**, 281.

NAKAMURA, H. & KURODA, K. 1937 *Keijo J. Med.* **8**, 256.

PONDER, E. 1925 *Q. J. Exp. Physiol.* **15**, 235.

PROBSTEIN, R. F., YUNG, D. & HICKS, R. E. 1977 Paper presented at Theory, Practice and Process Principles for Physical Separation, Eng. Foundation Conf., Asilomar, Calif.

SCHAFLINGER, U. 1984 *Intl J. Multiphase Flow* **11**, 189.

SCHNEIDER, W. 1982 *J. Fluid Mech.* **120**, 323.

SOKOLOV, W. J. 1971 *Moderne Industrizentrifugen*. VEB Verlag Technik.

SVAROVSKY, L. 1981 *Solid–Liquid Separation*, 2nd edn. Butterworths.

UNGARISH, M. & GREENSPAN, H. P. 1986 *J. Fluid Mech.* **162**, 117.

WENDROFF, B. 1972*a* *J. Math. Anal. Appl.* **38**, 454.

WENDROFF, B. 1972*b* *J. Math. Anal. Appl.* **38**, 640.

WHITHAM, G. B. 1974 *Linear and Nonlinear Waves*. Wiley.